Human RNA Methyltransferase BCDIN3D Regulates MicroRNA Processing

Blerta Xhemalce,[1,2] Samuel C. Robson,[1] and Tony Kouzarides[1,*]
[1]Wellcome Trust/Cancer Research UK Gurdon Institute, The Henry Wellcome Building of Cancer and Developmental Biology, University of Cambridge, Tennis Court Road, Cambridge CB2 1QN, UK
[2]Institute for Cellular and Molecular Biology, College of Natural Sciences, University of Texas at Austin, 2506 Speedway, Stop A5000, Austin, TX 78712, USA
*Correspondence: t.kouzarides@gurdon.cam.ac.uk
http://dx.doi.org/10.1016/j.cell.2012.08.041

SUMMARY

MicroRNAs (miRNAs) regulate key biological processes and their aberrant expression may lead to cancer. The primary transcript of canonical miRNAs is sequentially cleaved by the RNase III enzymes, Drosha and Dicer, which generate 5′ monophosphate ends that are important for subsequent miRNA functions. In particular, the recognition of the 5′ monophosphate of pre-miRNAs by Dicer is important for precise and effective biogenesis of miRNAs. Here, we identify a RNA-methyltransferase, BCDIN3D, that O-methylates this 5′ monophosphate and negatively regulates miRNA maturation. Specifically, we show that BCDIN3D phospho-dimethylates pre-miR-145 both in vitro and in vivo and that phospho-dimethylated pre-miR-145 displays reduced processing by Dicer in vitro. Consistently, BCDIN3D depletion leads to lower pre-miR-145 and concomitantly increased mature miR-145 levels in breast cancer cells, which suppresses their tumorigenic phenotypes. Together, our results uncover a miRNA methylation pathway potentially involved in cancer that antagonizes the Dicer-dependent processing of miR-145 as well as other miRNAs.

INTRODUCTION

MicroRNAs (miRNAs) are short single-stranded RNA molecules (18–24 nucleotides) that posttranscriptionally interfere with gene expression in a variety of eukaryotes (Ghildiyal and Zamore, 2009). miRNAs target the RNA interference effector complex (RISC) to specific messenger RNAs (mRNAs) through partial base-paring to sequences predominantly found in the 3′ untranslated region (3′UTR). This interaction results in decreased translation of the proteins they encode and/or in the degradation of the mRNAs themselves (Fabian et al., 2010). To date, over 1,000 human miRNAs have been identified, and each of them potentially regulates many mRNAs (Friedman et al., 2009; Kozomara and Griffiths-Jones, 2011). Consequently, miRNAs have

been involved in numerous cellular processes, including development, differentiation, proliferation, apoptosis, the stress response, and viral defense (Fabian et al., 2010). Importantly, altered expression of miRNAs is a common trait of cancers (Farazi et al., 2011). Indeed, deciphering regulation of miRNA expression may be important not only for diagnostic, but also for therapeutic purposes (Kasinski and Slack, 2011). Due to the way that miRNAs are generated, their expression can be regulated at different levels. The first level is transcriptional as miRNAs are synthesized from larger transcripts by RNA polymerase II or RNA polymerase III complexes. The next level is posttranscriptional, as these primary miRNA precursors (pri-miRNA) undergo at least three steps before the mature single-stranded form. The pri-miRNA is first cleaved by Drosha to release a hairpin-loop-shaped RNA called pre-miRNA (Lee et al., 2003). The loop of this pre-miRNA is further cleaved by Dicer to generate a miRNA duplex (Chendrimada et al., 2005). The miRNA duplex is dissociated, and the passenger strand is discarded, whereas the guide strand is loaded onto the Argonaute (Ago) protein to form an active RISC complex (Kawamata and Tomari, 2010). Each of these steps is potentially subjected to regulation because the rate of transcription of a given pri-miRNA does not always correlate with the levels of its mature miRNA (Thomson et al., 2006). One crucial aspect of this process is related to the 5′ terminal end of these RNA molecules. Both RNase III enzymes, Drosha and Dicer, generate 5′ ends that contain a negatively charged monophosphate group. This 5′ monophosphate is bound by specific positively charged pockets in Dicer and Ago2, and these interactions are necessary for efficient and accurate processing as well as the stability of the mature RISC complex (Frank et al., 2010; Kawamata et al., 2011; Park et al., 2011). Here, we unveil an unexpected posttranscriptional modification of the 5′ monophosphate group. Specifically, we show that the previously uncharacterized human enzyme BCDIN3D O-methylates both in vitro and in vivo the 5′ terminal monophosphate group of the precursor of miR-145, resulting in a complete loss of its negative charge. Consistent with the importance of this charge for interaction with Dicer, methylated pre-miR-145 displays reduced processing by Dicer in vitro. Accordingly, upon BCDIN3D depletion, the association of Dicer with the product of pre-miR-145 processing increases in vivo. As a result, depletion of BCDIN3D in human cells leads to lower levels of pre-miR-145 and a concomitant increase of mature

miR-145. Our results also indicate that this is not limited to miR-145 but may be responsible for the regulation of many other miRNAs. Finally, the interest of our findings is further enhanced by the potential involvement of BCDIN3D in cancer, as BCDIN3D depletion in breast cancer cells abolishes their tumorigenic phenotypes. Altogether our results uncover a human enzyme defining a miRNA methylation pathway that antagonizes the Dicer-dependent processing of miRNAs and that has potential as a therapeutic target in cancer.

RESULTS

BCDIN3D Is a Methyltransferase that Targets the 5′ Monophosphate of Nucleic Acids

Methylation of DNA and specific residues within histones plays a crucial role in the epigenetic regulation of chromatin-based processes, such as transcription and genomic organization (Goldberg et al., 2007; Klose and Bird, 2006; Kouzarides, 2007; Xhemalce et al., 2011). With the aim of identifying novel epigenetic regulators, we set up a screen for previously uncharacterized methyltransferases that target chromatin. Among our candidates were BCDIN3 and BCDIN3D, the human members of the Bin3 family of putative methyltransferases. Members of this family are found from *Schizosaccharomyces pombe* to humans and share homology within their putative S-adenosyl Methionine (SAM) binding motif (Figure 1A). The two paralogs exist from *Drosophila melanogaster* to humans, whereas lower eukaryotes possess only one Bin3 family member (Figure 1B).

We assessed the activity of purified candidate proteins by using in vitro methyltransferase assays with purified histones and nucleosomes as substrates and ^{3}H-radioactive SAM as the methyl group donor. In our assays, BCDIN3D, but not BCDIN3, showed a specific activity in the form of a radioactive band migrating at the level of histone H3 (around 17 kDa) in a SDS-PAGE gel only in the presence of nucleosomes (Figure 1C). In order to test whether BCDIN3D was targeting the tail of histone H3, we repeated the methyltransferase assay with nucleosomes in which histone H3 carried a truncation of its 31 N-terminal amino acids (H3ΔNter). As shown in Figure 1D, the radioactive band did not disappear nor changed its migration in the H3ΔNter nucleosomes, suggesting that the methylated product was not histone H3. As the only material difference between histones and nucleosomes was the DNA-601 used to assemble the nucleosomes (Huynh et al., 2005), it was possible that the methylation product was the DNA-601 itself. Staining of the SDS-PAGE gel with ethidium bromide showed that the 601-DNA does migrate in an SDS PAGE gel forming a band around 17 KDa (Figure 1E). Moreover, BCDIN3D was able to methylate the 601-DNA in the absence of any histone (Figure 1F). However, BCDIN3D did not target the canonical cytosines within CpG sites because the methylation product was still observed when the 601-DNA was premethylated to saturation with the bacterial SspI enzyme that methylates these sites (Figure 1F). Rather, BCDIN3D targeted the 5′ monophosphate generated by the EcoRV digestion used during the 601-DNA purification procedure because the methylation product was no longer observed when the 601-DNA was pretreated with alkaline phosphatase (Figure 1F). Importantly, the methyltransferase activity was

intrinsic to BCDIN3D as point mutations in its SAM binding domain abolished its observed activity in our assay (Figures 1A and 1F). While we were performing these experiments, the homolog of BCDIN3D, BCDIN3, was reported to stabilize the nuclear noncoding RNA 7SK by methylating its 5′ γ-phosphate (Jeronimo et al., 2007; Shuman, 2007). In addition, we established that BCDIN3D is localized in the cytoplasm (Figures S1A–S1C available online). Finally, the activity that we observed on the 601-DNA was weak, i.e., the methylation reactions were at the limit of detection by liquid scintillation, and we needed to expose the radioactive gels on film for 2–4 weeks in order to detect a significant signal. Based on these observations, we hypothesized that the bona fide target(s) of BCDIN3D may be RNA(s) that are monophosphorylated at their 5′ end(s) as shown in Figure 1G.

BCDIN3D Affects the Levels of Precursor and Mature Forms of miR-145

We considered that micro RNAs (miRNA) were good candidates for being BCDIN3D targets. Indeed, although most primary precursors of miRNAs (pri-miRNA) are transcribed by RNA polymerase II and are 7-methyl-guanosine-capped, both the precursor miRNAs (pre-miRNA) generated by Drosha and the mature miRNAs generated by Dicer have 5′ monophosphate ends (Sarnow et al., 2006).

We first sought to determine a cellular system in which to identify the targets of BCDIN3D methylation. Because of global mRNA expression data linking BCDIN3D to breast cancer (Liu et al., 2007), we analyzed the role of BCDIN3D in a number of cellular assays relevant to this cancer. Cells from the triple negative breast cancer cell line MDA-MB-231 have the ability to grow in anchorage-independent conditions, a hallmark of cell transformation, and to penetrate through a basement membrane matrix, a key property of cellular invasion. Stable shRNA-mediated depletion of BCDIN3D in these cells reduced their ability to form colonies in soft agar medium (anchorage-independent growth assay, Figure 2A). Moreover, depletion of BCDIN3D by using this shRNA and another siRNA targeting an independent sequence of BCDIN3D (Figure S3A) significantly decreased the invasiveness of the MDA-MB-231 cells (invasion assay, Figure 2D and Figures S2C and S2D) without greatly affecting their growth and migration abilities (growth assay, Figure 2B; MTT assay, Figure S2A and migration assay, Figure 2C and Figure S2B). Importantly, reintroduction of an shResistant BCDIN3D-GFP protein into the cells expressing shBCDIN3D at levels similar to the endogenous BCDIN3D protein (Figure 2E) fully rescued the invasion defect of these cells (Figure 2F), clearly demonstrating that the observed effects are specific.

Having confirmed the relevance of BCDIN3D in breast cancer cells, we depleted BCDIN3D in the MCF-7 breast cancer cell line and monitored its effect on the levels of five mature miRNAs (miR-10b, miR-21, miR-125b, miR-145, and miR-155) that are known to be consistently deregulated in breast cancer (Iorio et al., 2005). As shown in Figure 3A, MCF-7 cells transfected with an siRNA targeting the first exon of BCDIN3D (siBCDIN3D, depletion efficiency shown in Figure S1B and Figure S3B) displayed significantly increased levels of mature miR-145 compared to MCF-7 cells transfected with nontargeting negative
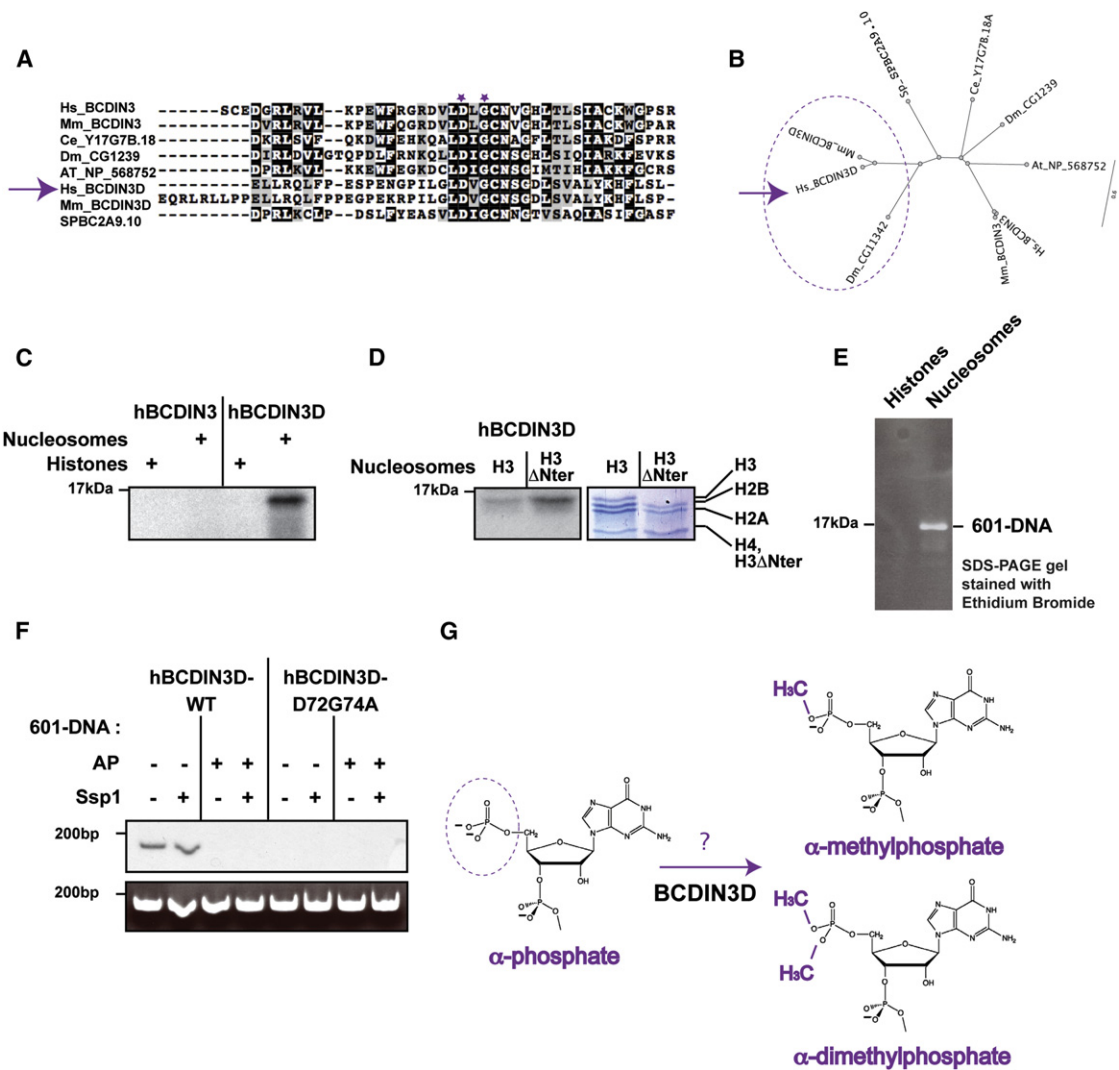
Figure 1. BCDIN3D Is a Methyltransferase that Targets the 5′ Monophosphate of Nucleic Acids

(A) Alignment of the SAM binding domain of the Bin3 family members from *S. pombe, Arabidopsis thaliana, C. elegans, D. melanogaster, Mus musculus* and *Homo sapiens*, generated with the CLUSTAL W algorithm. The asterisks indicate the residues that, when mutated to Alanine, abolish the methyltransferase activity of human BCDIN3D (F). The arrow indicates human BCDIN3D.

(B) Phylogenetic tree based on the alignment shown in (A), generated with the Geneious software. The dashed ellipsoid underlines the BCDIN3D cluster and the arrow indicates human BCDIN3D.

(C) In vitro methyltransferase assay with recombinant human BCDIN3 and BCDIN3D, ³H-radioactive SAM as methyl group donor, and either histones or nucleosomes as substrate. The reactions were loaded on a 15% SDS-PAGE gel, fixed, and subjected to autoradiography. The radioactive band observed in the BCDIN3D/nucleosome lane comigrates with histone H3.

(D) In vitro methyltransferase assay with recombinant BCDIN3D, ³H-SAM, and nucleosomes, in which histone H3 is either full length (H3) or is truncated of the 31 first amino-acids (H3ΔNter). The truncation makes H3ΔNter migrate faster (Coomassie staining, right), but does not modify the migration of the radioactive band (autoradiography, left).

(E) One microgram of histones and nucleosomes were loaded on a 15% SDS-PAGE gel and stained with ethidium bromide. The band observed in the nucleosome lane corresponds to the 601-DNA used to assemble the nucleosomes.

(F) In vitro methyltransferase assay using recombinant human BCDIN3D-WT and BCDIN3D-D72G74A catalytic mutant, ³H-radioactive SAM as methyl group donor and purified 601-DNA as substrate. The 601-DNA is generated by cleavage from a plasmid harboring multiple tandem repeats of the sequence flanked by EcoRV restriction sites. Prior to the methyltransferase assay with BCDIN3D, the 601-DNA was either CpG methylated by using the Ssp1 bacterial methyltransferase and/or treated with alkaline phosphatase (AP) that removes the 5′-alpha-phosphate left from the EcoRV digestion. The DNA from the methyltransferase assays with BCDIN3D was purified, loaded on a native 6% PAGE gel, stained with ethidium bromide (lower), fixed, and subjected to autoradiography (upper).

(G) Schematic representing the inferred methyltransferase activity of BCDIN3D on a 5′ monophosphorylated ribonucleotide. The dashed ellipsoid underlines the 5′-alpha-phosphate group.
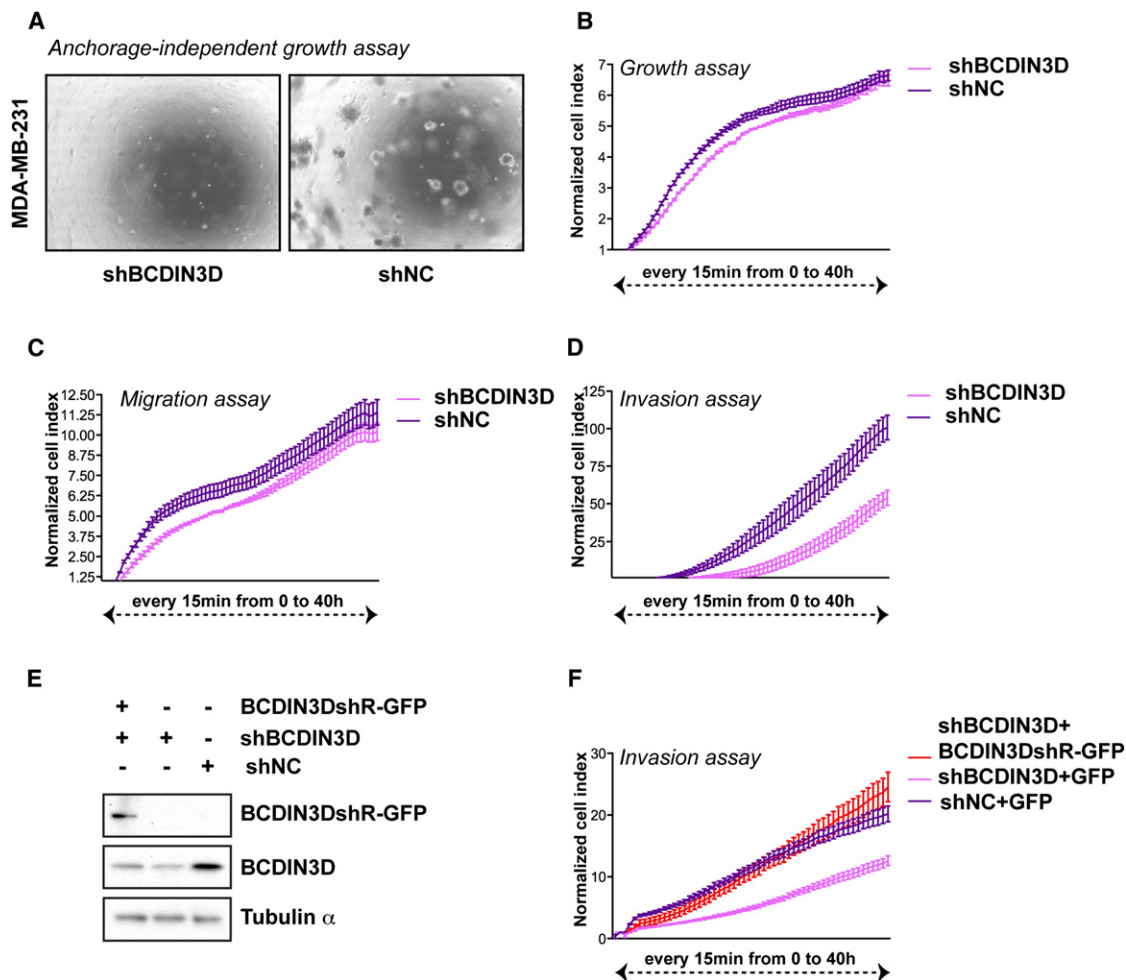
See also Figure S1.

Figure 2. BCDIN3D Depletion Suppresses Tumorigenic Phenotypes In Vitro

(A) Stable depletion of BCDIN3D in the MDA-MB-231 breast cancer cells abolishes anchorage-independent growth. Microscopic image of MDA-MB-231 [shBCDIN3D] and MDA-MB-231 [shNC] cells growing in soft agar after 4 weeks incubation (see Extended Experimental Procedures for further detail).

(B–D) Stable BCDIN3D depletion substantially impairs invasiveness, but not growth and migration, of MDA-MB-231 cells. MDA-MB-231 [shBCDIN3D] and MDA-MB-231 [shNC] cells were analyzed with the xCELLigence system, which allows to assess cellular growth (B, growth assay), migration through a 8 μM pore size membrane (C, migration assay) or invasion through a 8 μM pore size membrane coated with Matrigel (D, invasion assay) in parallel and in real time. The cells were trypsinized and loaded in quadruplets onto an E-plate (B, growth assay), CIM-plate (C, migration assay) or CIM-plate coated with 1/40 dilution of Matrigel (D, invasion assay). The cell index was measured every 15 min for 48 hr. The results of the assay are represented as normalized cell index. Error bars represent SEM values.

(E) MDA-MB-231 [shBCDIN3D+BCDIN3DshR(esistant)-GFP] express BCDIN3DshR-GFP at levels similar to endogenous BCDIN3D protein. MDA-MB-231 [shBCDIN3D+BCDIN3DshR-GFP], MDA-MB-231 [shBCDIN3D+GFP], and MDA-MB-231 [shNC+GFP] cell lines were generated as indicated in the Extended Experimental Procedures. Whole-cell extracts were analyzed by western blot with anti-BCDIN3D antibody and the loading control alpha-tubulin. The two panels showing the endogenous and BCDIN3DshR-GFP are from the same exposure of the same blot.

(F) Expression of BCDIN3DshR-GFP in MDA-MB-231 [shBCDIN3D] cell lines suppresses their invasion defect. The MDA-MB-231 [shBCDIN3D+BCDIN3DshR-GFP], MDA-MB-231 [shBCDIN3D+GFP]. and MDA-MB-231 [shNC+GFP] cell lines were analyzed as in (B–D) and the invasion assays are shown. Error bars represent SEM values.

See also Figure S2.

control siRNAs (siNC). A similar increase in mature miR-145 levels was observed when MCF-7 cells were transfected with an independent pool of siRNAs targeting the second exon of BCDIN3D (Figures S3A–S3C). Moreover, a milder but reproducible increase of mature miR-145 levels was observed in MDA-MB-231 cells transfected with siBCDIN3D compared to cells transfected with siNC (Figure S3D) or the MDA-MB-231 cells stably expressing shBCDIN3D compared to those expressing shNC or shBCDIN3D rescued with the BCDIN3DshR-GFP construct (Figure S3E). Importantly, the results obtained by quantitative reverse transcription and PCR (qRT-PCR) were confirmed by northern blot with a probe against miR-145 in the nontransformed but immortalized BJ+TERT cells that express higher levels of miR-145 than MCF-7 cells (Figures S3F and
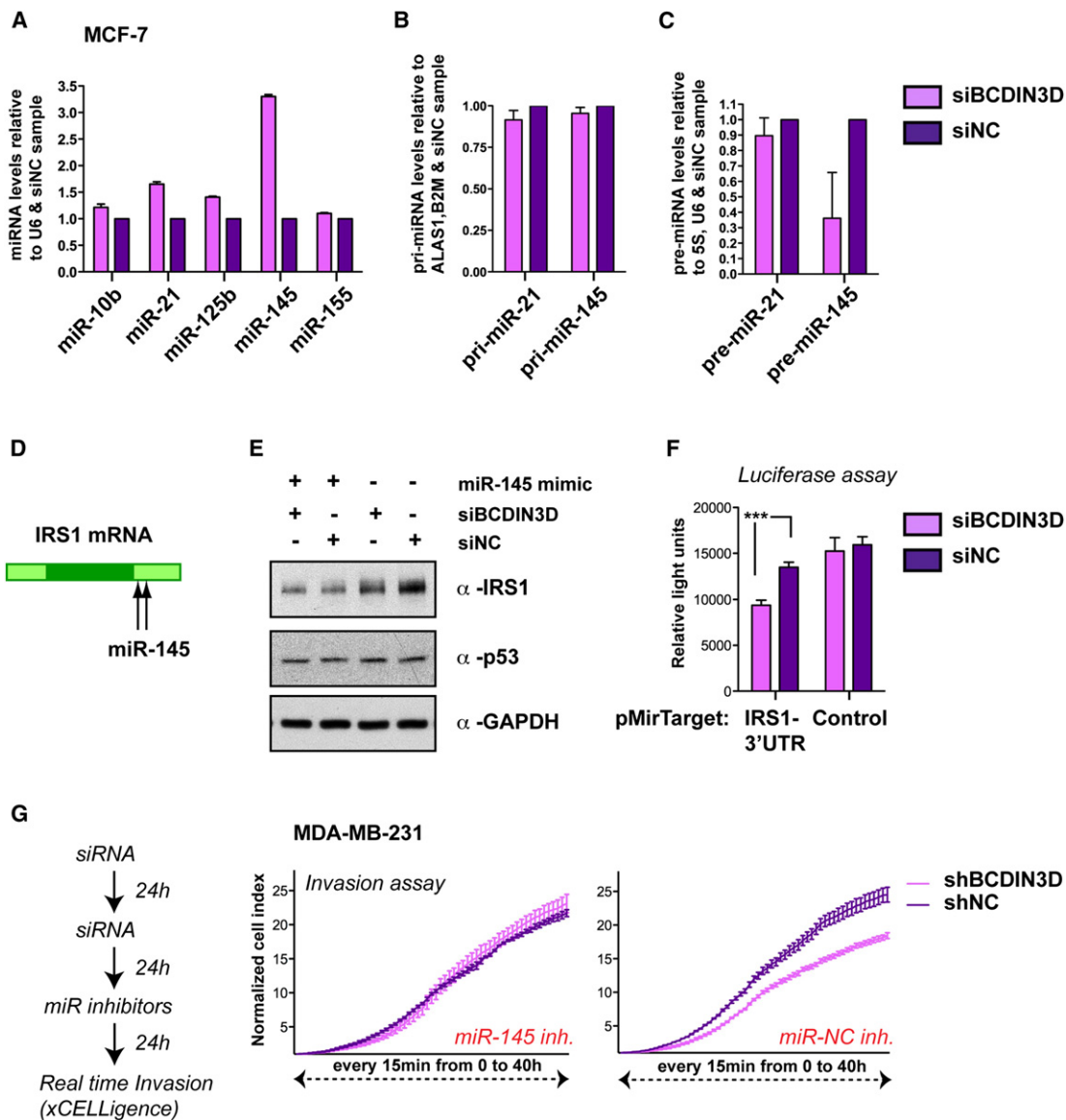
Figure 3. siRNA-Mediated Depletion of BCDIN3D Changes the Levels of Precursor and Mature Forms of miR-145

MCF-7 cells were transfected with a siRNA targeted against the first exon of BCDIN3D (siBCDIN3D) or with non targeting siRNAs as a negative control (siNC).

(A) The levels of the indicated miRNAs were analyzed by quantitative reverse transcription and PCR (qRT-PCR) analysis. The data are normalized to the U6 RNA and to siNC cells. Error bars represent SEM values.
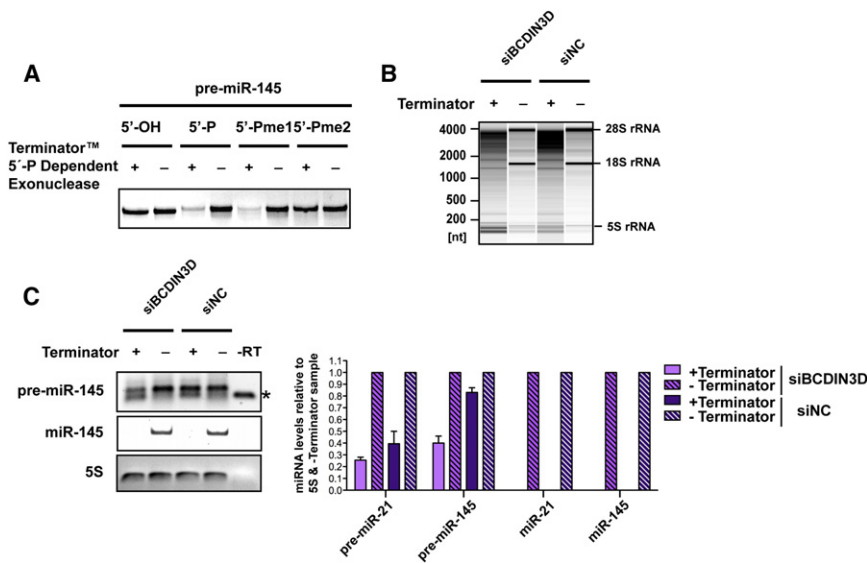
(B) Transcript levels of the pri-miR-145 were not significantly altered upon BCDIN3D depletion. The pri-miRNA levels were analyzed by qRT-PCR and normalized to the ALAS1 and B2M mRNAs and to siNC cells. Error bars represent SEM values.

(C) The levels of pre-miR-145 are reduced upon BCDIN3D depletion. The pre-miRNA levels were analyzed by qRT-PCR and normalized to the 5S and U6 RNAs and to siNC cells. Error bars represent SEM values.

(D) Schematic view of the IRS-1 mRNA and the sequences targeted by miR-145.

(E) In a similar manner to miR-145 overexpression, BCDIN3D depletion affects IRS-1 expression at the protein level. These effects are not due to p53 stabilization. MCF-7 cells were cotransfected with miR-145 mimic, siBCDIN3D, and siNC as indicated and analyzed by western blot with antibodies against IRS-1, p53 and the loading control GAPDH.

(F) BCDIN3D depletion significantly reduces the expression of the luciferase reporter gene fused to the 3′UTR of the IRS-1 mRNA. siBCDIN3D and siNC transfected MCF-7 cells were transfected with pMirTarget (Origene) containing or not the 3′-UTR of IRS1 fused to the luciferase reporter gene and after 24 hr, the cells were lysed and the luciferase activity was measured in a luminometer. Shown are results from a typical experiment in quadruplets. Error bars represent SEM values. The transfection efficiency of the plasmids, as assessed by the expression of RFP gene contained in the pMirTarget plasmid, was identical in all samples.

(G) miR-145 inhibition rescues the invasion defect of MDA-MB-231 cells transfected with siBCDIN3D. MDA-MB-231 were transfected according to the procedure schematized on the left with siRNAs against BCDIN3D and negative control, followed by anti miR-145 inhibitors and negative control. Twenty-four hours after the transfection of the miRNA inhibitors, the cells were trypsinized and analyzed as in Figures 2B–2D; the invasion assays are shown. Error bars represent SEM values. See also Figure S3.

Figure 4. BCDIN3D Dimethylates the 5′ Phosphate Group of (Pre-)miR-145 In Vitro

(A) BCDIN3D preferentially methylates pre-miR-145. In vitro methyltransferase assay using recombinant GST-BCDIN3D (1–8) or GST (9–10), ^{3}H-radioactive SAM as methyl group donor and the following synthetic DNA and RNA molecules as substrate (1) deoxy-pre-miR-145 [5′-OH]; (2) deoxy-pre-miR-145 [5′-P]; (3&9) pre-miR-145 [5′-OH]; (4 and10) pre-miR-145 [5′-P]; (5) duplex miR-145 [5′-P]; (6) miR-145 [5′P]; (7) miR-145* [5′P]; and (8) mock. The nucleic acids were purified and analyzed by autoradiography (left) and liquid scintillation (right). Error bars represent SD values. Full recovery of nucleic acids after purification was verified with a spectrophotometer.

(B–D) The product of BCDIN3D methylation is a 5′ phospho-dimethyl. (B) In vitro methyltransferase assay as in (A) using as substrate synthetic pre-miR-145 molecules that have [5′-OH], [5′-P], [5′-Pme1] or [5′-Pme2] ends (see Figure 1G). Lower panel shows the Staining with ethidium bromide of the gel used for the autoradiography shown in the upper panel. (C) Synthetic pre-miR-145 molecules that have [5′-OH], [5′-P], [5′-Pme1] or [5′-Pme2] ends were ligated with the T4 RNA Ligase 1. The circular RNA molecules migrate faster than the linear molecules. pre-miR [5′-Pme2] is resistant to ligation. (D) Synthetic pre-miR-145 [5′-P] was in vitro methylated as in (A) prior to ligation with T4 RNA Ligase 1. Left panel shows the ethidium bromide staining of the gel used for the autoradiography shown in the right panel. The pre-miR-145 molecules that were methylated by BCDIN3D were also resistant to ligation.

S3G). Interestingly, the levels of pri-miR-145 were not increased upon BCDIN3D depletion (Figure 3B), whereas the levels of pre-miR-145 were significantly decreased (Figure 3C). This suggested that the upregulation of miR-145 was not due to a transcriptional effect but rather to a downstream effect on either the processing of miR-145 and/or its stability.

The increase in the levels of mature miR-145 seen after BCDIN3D depletion resulted in several expected functional consequences. Indeed, similar to miR-145 overexpression, BCDIN3D depletion decreased the levels of IRS1, a previously established miR-145 target (Shi et al., 2007; Spizzo et al., 2010), at both the protein and RNA levels (Figures 3D and 3E and data not shown) and significantly reduced the expression of the luciferase reporter gene fused to the 3′UTR of the IRS1 mRNA (Figure 3F). Moreover, the miR-145 motif was significantly enriched (p = 0.0026) in the 3′UTR of genes downregulated upon BCDIN3D depletion, whereas the other four miRNAs tested were not (see below). Finally, despite the apparently mild increase of miR-145 levels in MDA-MB-231 cells transfected with siBCDIN3D compared to siNC (Figure S3D), the transfection of miR-145 inhibitors totally or partially rescued the invasion defect of these cells, depending on the density of the matrigel (Figure 3G and data not shown). Altogether, these results strongly suggest that BCDIN3D regulates mature miR-145 levels and that miR-145 is a functional mediator of the phenotypic effects of BCDIN3D depletion.

BCDIN3D Dimethylates the 5′ Phosphate Group of (Pre-)miR-145 In Vitro

To test whether miR-145 is a direct target of BCDIN3D activity, we performed in vitro methyltransferase assays by using recombinant BCDIN3D and synthetic forms of miR-145 and ^{3}H-SAM, and analyzed them by autoradiography and liquid scintillation counting. In these assays, BCDIN3D showed a strong activity and a preference for the precursor form of miR-145 (pre-miR-145) compared to either the double-stranded miR-145 or the single-stranded miR-145 and its passenger miR-145* (Figure 4A). Importantly, BCDIN3D did not methylate the 5′OH unphosphorylated form of neither pre-miR-145, miR-145, or miR-145* (Figure 4A and data not shown), validating the specificity of BCDIN3D activity toward the 5′ monophosphate. Finally, BCDIN3D could not methylate the 5′P deoxy-ribonucleotide form of pre-miR-145 confirming that BCDIN3D has indeed a preference for RNA molecules (Figure 4A).

As illustrated in Figure 1G, the 5′ monophosphate group contains two negatively charged oxygen moieties [-O$^-$] that can be subject to methylation [-O-CH$_3$]. We therefore sought to determine whether BCDIN3D methylates one or both available oxygen moieties. To this purpose, we synthesized pre-miR-145 molecules in which the 5′ monophosphate group was either mono- (5′Pme1) or dimethylated (5′Pme2). We first submitted them to in vitro methyltransferase assays with recombinant

Figure 5. Pre-miR-145 Is Also Modified in a BCDIN3D-Dependent Manner In Vivo

(A) Synthetic pre-miR-145 molecules that have [5′-OH], [5′-P], [5′-Pme1], or [5′-Pme2] 5′ ends were treated with Terminator 5′-P-dependent exonuclease that is a processive 5′-3′ exonuclease that digests RNAs having a 5′ monophosphate. Pre-miR [5′-Pme2] is resistant to this treatment.

(B) RNA from MCF-7 cells treated or not with Terminator was migrated on an Agilent Total Eukaryotic RNA pico Chip. The treatment was specific as the Terminator fully digested the 18S and 28S rRNA, which have 5′ monophosphates but did not digest the 5S RNA, which has a 5′ triphosphate.

(C) RNA treated as in (B) was analyzed by reverse transcription and PCR with primers specific for pre-miR-21, pre-miR-145, miR-21, miR-145, and 5S. The 5S RNA is known to be 5′ triphosphate and is used to control for equal RNA recovery. The indicated RNAs were analyzed by quantitative RT-PCR and normalized to the 5S RNA and to the [-Terminator] sample (graph on right). Error bars represent SEM values. To facilitate the visualization of the assay, the PCRs were also analyzed by semiquantitative PCR (left). For each primer, the semiquantitative PCRs were performed in parallel with the quantitative PCRs and were stopped at the same cycle as the quantitative PCR reached the threshold of the less abundant sample. The treatment with Terminator fully digests miR-145 but not pre-miR-145. The asterisk indicates a nonspecific band.

See also Figures S4, S5, and S6.

BCDIN3D and ³H-radioactive SAM. BCDIN3D could still methylate pre-miR-145 [Pme1] but not pre-miR-145 [Pme2] (Figure 4B), strongly suggesting that BCDIN3D can methylate both oxygen moieties of the 5′ monophosphate end. In order to determine the ratio of mono- and dimethylated 5′ monophosphate products in our in vitro methyltransferase assays, we exploited the enzymatic properties of T4 RNA Ligase 1. This enzyme catalyzes the ligation of a 5′ monophosphate nucleic acid donor to a 3′ hydroxyl-terminated nucleic acid acceptor through the formation of a 3′→5′ phosphodiester bond. As expected, the ligation reaction circularized the synthetic pre-miR-145 5′ monophosphate RNA molecule resulting in a faster migrating band (Figure 4C). In our conditions, T4 RNA Ligase 1 could still efficiently ligate pre-miR-145 [Pme1] but not pre-miR-145 [Pme2], thus providing us with a tool to discriminate between the mono- and the dimethylated forms of the 5′ monophosphate end (Figure 4C). As shown in Figure 4D, pre-miR-145 methylated with BCDIN3D (radioactive band on the right) was fully resistant to ligation with T4 RNA Ligase 1, indicating that the product of BCDIN3D methylation is a 5′Pme2.

Pre-miR-145 Is Modified by BCDIN3D In Vivo

To determine whether BCDIN3D also targets miR-145 and/or its precursor in vivo, we set up an assay that takes advantage of the fact that the 5′Pme2 end is also resistant to treatment with the Terminator 5′ Phosphate-Dependent Exonuclease that specifically digests RNAs having a 5′ monophosphate (Figure 5A). We treated RNA purified from MCF-7 cells transfected with siBCDIN3D and siNC with the Terminator enzyme and analyzed the resulting RNAs by quantitative reverse transcription and PCR with specific primers for pre-miR-145 and miR-145 as well as controls (Figures 5B and 5C). To verify that the treatment with Terminator was effective, the RNAs, treated

with either Terminator or mock, were analyzed by electrophoresis on an Agilent Total RNA Pico chip. As shown on Figure 5B, Terminator fully digested the 28S and 18S rRNAs, which have 5′ monophosphate ends but left intact the 5S rRNA, which has a 5′ triphosphate end. The treatment also fully digested miR-21, which is known to be monophosphate (Affymetrix ENCODE Transcriptome Project, 2009) (Figure 5C). Under these conditions, a significant proportion of pre-miR-145, but not miR-145, was resistant to digestion with Terminator in siNC transfected MCF-7 cells (Figure 5C). Moreover, the Terminator resistant fraction of pre-miR-145 was significantly reduced in siBCDIN3D-treated MCF-7 cells (Figure 5C). This shows that the 5′end of pre-miR-145 is modified in a BCDIN3D-dependent manner in vivo. Together with the in vitro activity of BCDIN3D on pre-miR-145, this suggests that pre-miR-145 is dimethylated at its terminal 5′ monophosphate. Interestingly, a smaller portion of pre-miR-21 was also resistant to Terminator suggesting that miR-21 is also a BCDIN3D target. This could explain the mild increase of the mature levels of miR-21 in some of our assays.

Our global whole RNA analysis in siBCDIN3D and siNC-treated MCF-7 cells also suggested that miR-145 is not the only target of BCDIN3D. Indeed, mRNAs downregulated in siBCDIN3D cells were very significantly enriched with multiple putative miRNA targeting sequences (Figure S4 and Extended Experimental Procedures). Moreover, we found additional miRNAs whose expression is increased in siBCDIN3D compared to siNC cells through miRNA profiling with the miRCURY LNA PCR platform from Exiqon (Figure S5 and Extended Experimental Procedures). In particular, we determined that the precursor of miR-23b was also modified in a BCDIN3D-dependent manner in vivo (Figure S5D) and in vitro (Figure S6), indicating that BCDIN3D robustly modifies other miRNA targets.
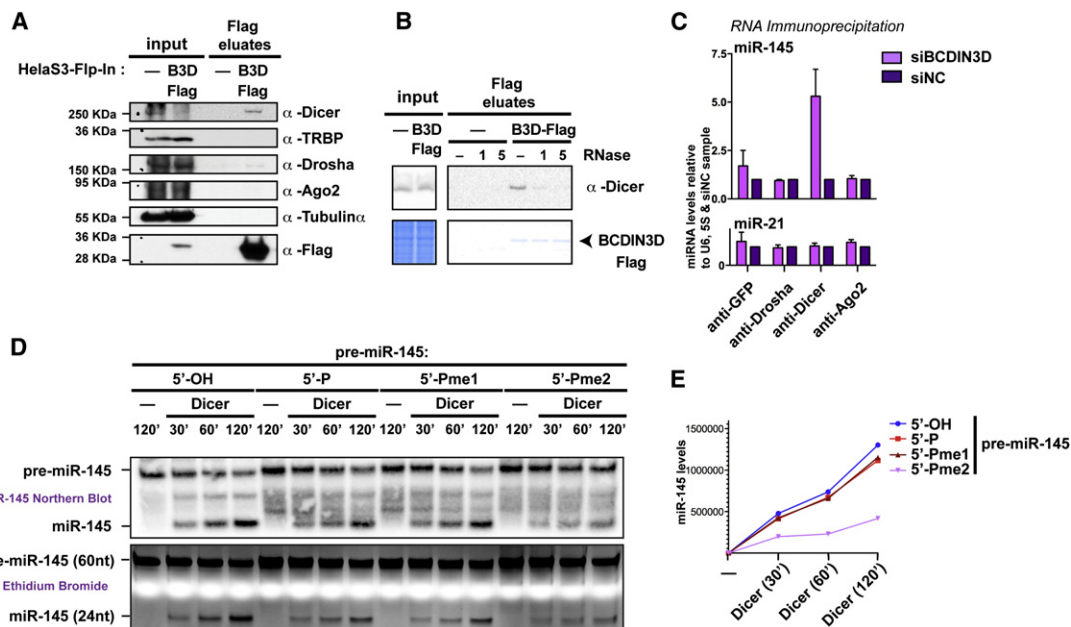
Figure 6. BCDIN3D Interacts with Dicer and Its Depletion Affects miR-145 Association with Dicer

(A) BCDIN3D specifically interacts with Dicer. Flag eluates from isogenic HELA-S3-Flp-In (-) and HELA-S3-Flp-In-BCDIN3D-Flag (BCDIN3D-Flag) stable cell lines coimmunoprecipitated with an anti-Flag antibody were analyzed by western blotting with the indicated antibodies (see Extended Experimental Procedures for further detail).

(B) The interaction between BCDIN3D and Dicer is sensitive to treatment with RNase A. Flag co-IPs were performed as in (A) in the presence of mock or 1 or 5 μl of RNase A (see Extended Experimental Procedures for further detail). The co-IPs were analyzed by Coomassie staining to confirm equal recovery of BCDIN3D (lower) and by western blot with the Dicer antibody (upper).

(C) Upon BCDIN3D depletion, the association of Dicer with miR-145, the product of pre-miR-145 processing, is significantly increased. MCF-7 cells transfected with siBCDIN3D or siNC were subjected to RNA-immunoprecipitation with the indicated antibodies (see Extended Experimental Procedures for further detail). RNA from the immunoprecipitates was purified and the levels of miR-21 and miR-145 were analyzed by qRT-PCR. The data are normalized to the 5S and U6 RNAs and to siNC cells. Error bars represent SEM values.

(D and E) Synthetic pre-miR-145 molecules that have [5'-OH], [5'-P], [5'-Pme1], or [5'-Pme2] 5' ends were incubated with human Dicer or mock at 1 mM of MgCl2 for 30, 60 or 120 min as indicated (see Extended Experimental Procedures for further detail). The Dicer processing reactions were loaded on a 15% Urea-PAGE gel and stained with ethidium bromide. The gel was photographed with the Chemidoc XRS+ system from Biorad (D, lower) and analyzed by northern blot with an anti-miR-145 probe (D, upper). The miR-145 product was quantified by using the Image Lab Software (E).

See also Figure S7.

BCDIN3D Affects miR-145 Association with Dicer

These results prompted us to determine at what step in the RNAi pathway BCDIN3D participates. To this end, we first probed for in vivo interactions between BCDIN3D and proteins involved in the RNAi pathway. We performed anti-Flag coimmunoprecipitations (co-IP) from HeLa-S3-Flp-In control and -BCDIN3D-Flag stable cell lines followed by elution with a Flag peptide. This procedure highly reduced nonspecific interactions as shown by the lack of Tubulin alpha in our co-IPs, a common contaminant of Flag-affinity purifications (Gregory et al., 2004) (Figure 6A). We reproducibly detected an interaction of BCDIN3D with Dicer but not with other proteins of the RNAi pathway (Figure 6A). Importantly, we could not detect an interaction between BCDIN3D and TRBP, which stably interacts with Dicer and participates in the processing of pre-miRNAs to mature miRNAs (Chendrimada et al., 2005) (Figure 6A). Interestingly, the observed interaction between BCDIN3D and Dicer is disrupted by treatment with RNase A (Figure 6B), suggesting that the interaction may be mediated through RNA(s). The binding of BCDIN3D to Dicer is an additional strong

indicator that BCDIN3D has a direct role in the processing of miRNAs.

The observed increase in the levels of miR-145 upon BCDIN3D depletion could be due to either increased processing of miR-145, to increased stability of the mature miR-145, or to both. In order to distinguish among these three possibilities, we determined how depletion of BCDIN3D affected the association of miR-145 with proteins involved with its processing from pri- to pre- to mature miRNA. We performed RNA immunoprecipitations (RIP) with specific antibodies against Drosha, Dicer, and Ago2 in MCF-7 cells treated with either siBCDIN3D or siNC. As shown in Figure 6C, depletion of BCDIN3D significantly and specifically increased the association of miR-145 with Dicer. This suggests that depletion of BCDIN3D augments the processing of pre-miR-145 by Dicer into miR-145. Surprisingly, BCDIN3D depletion did not increase miR-145 association with Ago2, although it mildly increased the association of Ago2 with miR-21, another lesser BCDIN3D target. This may be a direct consequence of the fact that miR-145 has a guanine at position 1. The structure of the MID domain of human Ago2 was recently
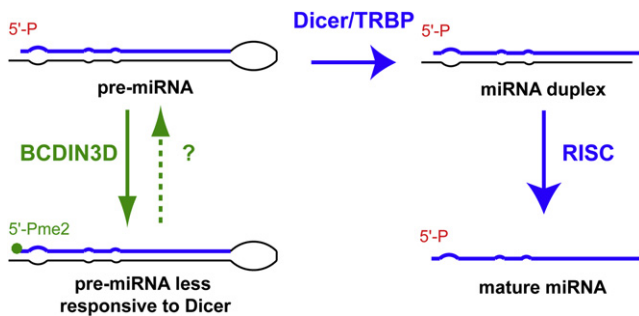
Figure 7. Model for the Mode of Action of BCDIN3D

solved and indicated that a loop within this domain discriminates against cytosines and guanines thereby lowering hAgo2 affinity for miRNAs that start with these residues (Frank et al., 2010). Another alternative albeit not exclusive explanation is that although the association of miR-145 with hAgo2 remains apparently unchanged, the increased association rate is actually compensated by a similarly increased dissociation rate.

The 5′ Phospho-Dimethyl Modification Reduces the Processing of Pre-miR-145 by Dicer

All of our results point to the fact that downregulation of BCDIN3D augments the Dicer-dependent processing of pre-miR-145 into miR-145. First, depletion of BCDIN3D leads to a reduction of pre-miR-145 levels and a concomitant increase of mature miR-145 levels (Figures 3A–3C). Second, upon BCDIN3D depletion, the association of Dicer with the product of pre-miR-145 processing increases (Figure 6C). Finally, we find that BCDIN3D modifies the pre- but not the mature miR-145 in vivo (Figure 5C), even though they have the same 5′end. Indeed, because the mature miR-145 is positioned on the 5p arm of the pre-miR-145 hairpin, the 5′end of the mature miR-145 is not produced by Dicer and is therefore the same as the 5′end of pre-miR-145. Together with the RIP results, this strongly suggests that the 5′ methylated pre-miR-145 molecules are not efficiently processed by Dicer in vivo. To test whether this effect is directly mediated by Dicer, we performed in vitro Dicer processing assays where human recombinant Dicer was incubated with synthetic pre-miR-145 molecules that have [5′-OH], [5′-P], [5′-Pme1] or [5′-Pme2] ends at physiological Mg^{2+} ions concentration (0.5–1 mM) (Günther, 2006). Under these conditions, the processing of pre-miR-145 [5′-Pme2] by Dicer was impaired compared to the other pre-miR-145 molecules (Figure 6D and Figure S7). The decrease in processing efficiency may result from the loss of the negative charge following methylation (Figure 1G) that in turn may affect the recognition of the 5′ monophosphate of the pre-miRNA by Dicer (Figure 7). This is supported by recent findings that human Dicer contains a basic motif that anchors the 5′ monophosphate terminus (Park et al., 2011).

DISCUSSION

Here we uncover an enzymatic activity mediated by human BCDIN3D, which methylates both oxygen moieties of a phosphate group on nucleic acids. Specifically, we show that BCDIN3D modifies the 5′ monophosphate end of miRNAs including pre-miR-145 and pre-miR-23b. Methylation of the 5′ monophosphate of pre-miRNAs by BCDIN3D inhibits their processing by Dicer. This inhibition is consistent with the recent finding that human Dicer possesses a basic motif that accommodates the negatively charged 5′ monophosphate of pre-miRNAs (Park et al., 2011). Importantly, the interaction between Dicer and the 5′ monophosphate is necessary for efficient and accurate processing of pre-miRNAs. (Park et al., 2011). Methylation of both oxygen moieties by BCDIN3D neutralizes the negative charges of the 5′ monophosphate group, This abrogation of charge may prevent the association of pre-miRNAs with the Dicer basic motif and result in the inhibition of Dicer activity. Together these findings suggest a model whereby direct methylation of pre-miRNAs by BCDIN3D generates a pool of pre-miRNAs that is less responsive to processing by Dicer (Figure 7). The fact that BCDIN3D can associate with Dicer (but not TRBP) may be an indication that BCDIN3D acts on miRNAs while complexed with Dicer. However, it is also possible that the interaction between Dicer and BCDIN3D functions in other aspects of this pathway.

BCDIN3D prefers RNA to DNA because the deoxy- form of pre-miR-145 is a far inferior substrate compared to its ribonucleotide counterpart (Figure 4A). Given that the 5′ monophosphate group is identical between these molecules, other features, such as tri-dimensional structure or the presence of uracil instead of thymine, could determine this specificity. Of course, the possibility remains that BCDIN3D could also target DNA, which may be revealed under specific conditions or biological processes. This notion is supported by an example from *Caenorhabditis elegans* where Dicer is converted from a ribonuclease to a deoxy-ribonuclease through the action of a caspase during apoptosis (Nakagawa et al., 2010).

miRNAs are involved in numerous cellular effects and often several miRNAs function in concert to regulate a given biological function. Because BCDIN3D regulates a subset of miRNAs, this enzyme may function in specific biological processes depending on the cellular and/or physiological context. One possible role of BCDIN3D in cancer cells may be to promote cellular invasion (Figure 2). This idea is consistent with the finding that BCDIN3D mRNA is overexpressed in highly tumorigenic breast cancer stem cells and BCDIN3D is included in an "invasiveness" gene signature (Liu et al., 2007). In addition, two established in vivo targets of BCDIN3D, pre-miR-145 and pre-miR23b, are able to suppress the process of cellular invasion (Sachdeva et al., 2009; Shi et al., 2007; Spizzo et al., 2010; Zhang et al., 2011). Collectively, these findings strongly suggest that the negative effect of BCDIN3D depletion on invasion could be due to its effects on several miRNAs. Indeed, a recent genome-wide functional screen showed that 69 out of 900 miRNAs tested were able to inhibit cellular invasion (Zhang et al., 2011). The potential of BCDIN3D to affect many miRNAs simultaneously may allow it to tightly control specific pathways, including cellular invasion. Future work should allow us to establish whether this effect may be explored for therapeutic targeting in breast and possibly other cancers.

EXPERIMENTAL PROCEDURES

The details of all siRNAs, synthetic RNAs, primers and antibodies used in the study are provided in Tables S1, S2 and S3. Extended Experimental Procedures are included in the Supplemental Information and/or are available upon request.

Knockdown Experiments

ON-TARGETplus siRNAs against BCDIN3D and control were purchased from Dharmacon and reverse-transfected in two rounds into MCF7, MDA-MB-231 or BJ+TERT cells by using Lipofectamine RNAiMAX from Invitrogen or HiPerfect from QIAGEN. miR-145 mimics and inhibitors were from Ambion. The MDA-MB-231 clones stably expressing shRNAs against BCDIN3D or control were generated by transfecting MDA-MB-231 cells with the pRS vectors containing 29-mer shRNA against BCDIN3D (TR317908, t1368843) and noneffective scrambled shRNAs (TR30012) from Origene respectively. The shBCDIN3D rescue clones were generated by transfecting tGFP-tagged BCDIN3D carrying a silent C324/C327A mutation.

Cellular Assays

For the soft agar colony assays, 3×10^4 cells were plated in 0.35% agar in complete growth medium in 6-well plates and colonies were analyzed after 4 to 5 weeks. The real-time growth, migration, and invasion assays were performed with the xCELLigence system from Roche following the manufacturer's instructions. A 1/40th dilution of Matrigel was used to coat the upper chamber of the CIM plate for the invasion assays.

RNA Analysis

Total RNA and proteins were extracted from the same cells by using the RNA/Protein purification kit from Norgen. 20–200 ng of total RNA was used for detection of miRNAs with the *mir*Vana qRT-PCR miRNA detection kit and/or the Taqman MicroRNA Reverse Transcription Kit from Applied Biosystems. Real-time PCR analysis was performed on a StepOne Plus system or Vii7A from Applied Biosystems. The northern blots were performed as previously described (Xhemalce and Kouzarides, 2010).

Modified RNAs

Precursor, mature, and passenger miR-145 carrying 5′OH, 5′P, 5′Pme1, or 5′Pme2 modifications were custom synthesized by IBA GmbH.

In Vitro RNA Methyltransferase Assays

These assays were performed in a total volume of 100 μl in 25 mM Tris-HCl [pH 8], 150 mM NaCl, 2 mM KCl, 10% glycerol, 1 mM EDTA, 1 mM DTT supplemented with EDTA-free Complete Protease Inhibitor cocktail from Roche, and 80 U of RNaseOUT from Invitrogen with 1 μg of recombinant BCDIN3D, 4 μl of 20 μM synthetic RNAs, and 4 μl of ^{3}H-SAM (PerkinElmer NET155250UC) for 2 hr at 37°C.

In Vitro Dicer Processing Assays

These assays were performed essentially as described (Park et al., 2011) with 100 pmol of synthetic pre-miRNA, 500 ng of recombinant human Dicer in a total volume of 15 μl in 100 mM KCl, 10 mM Tris-HCl [pH 8], 0.1 mM EDTA, 0.5 or 1 mM $MgCl_2$, 0.5 mM dTT supplemented with 0.5 U/μl RNaseOUT for the indicated times at 37°C.

SUPPLEMENTAL INFORMATION

Supplemental Information includes Extended Experimental Procedures, seven figures, and three tables and can be found with this article online at http://dx.doi.org/10.1016/j.cell.2012.08.041.

REFERENCES

Affymetrix ENCODE Transcriptome Project; Cold Spring Harbor Laboratory ENCODE Transcriptome Project. (2009). Post-transcriptional processing generates a diversity of 5′-modified long and short RNAs. Nature *457*, 1028–1032.

Chendrimada, T.P., Gregory, R.I., Kumaraswamy, E., Norman, J., Cooch, N., Nishikura, K., and Shiekhattar, R. (2005). TRBP recruits the Dicer complex to Ago2 for microRNA processing and gene silencing. Nature *436*, 740–744.

Fabian, M.R., Sonenberg, N., and Filipowicz, W. (2010). Regulation of mRNA translation and stability by microRNAs. Annu. Rev. Biochem. *79*, 351–379.

Farazi, T.A., Spitzer, J.I., Morozov, P., and Tuschl, T. (2011). miRNAs in human cancer. J. Pathol. *223*, 102–115.

Frank, F., Sonenberg, N., and Nagar, B. (2010). Structural basis for 5′-nucleotide base-specific recognition of guide RNA by human AGO2. Nature *465*, 818–822.

Friedman, R.C., Farh, K.K., Burge, C.B., and Bartel, D.P. (2009). Most mammalian mRNAs are conserved targets of microRNAs. Genome Res. *19*, 92–105.

Ghildiyal, M., and Zamore, P.D. (2009). Small silencing RNAs: an expanding universe. Nat. Rev. Genet. *10*, 94–108.

Goldberg, A.D., Allis, C.D., and Bernstein, E. (2007). Epigenetics: a landscape takes shape. Cell *128*, 635–638.

Gregory, R.I., Yan, K.P., Amuthan, G., Chendrimada, T., Doratotaj, B., Cooch, N., and Shiekhattar, R. (2004). The Microprocessor complex mediates the genesis of microRNAs. Nature *432*, 235–240.

Günther, T. (2006). Concentration, compartmentation and metabolic function of intracellular free Mg2+. Magnes. Res. *19*, 225–236.

Huynh, V.A., Robinson, P.J., and Rhodes, D. (2005). A method for the in vitro reconstitution of a defined "30 nm" chromatin fibre containing stoichiometric amounts of the linker histone. J. Mol. Biol. *345*, 957–968.

Iorio, M.V., Ferracin, M., Liu, C.G., Veronese, A., Spizzo, R., Sabbioni, S., Magri, E., Pedriali, M., Fabbri, M., Campiglio, M., et al. (2005). MicroRNA gene expression deregulation in human breast cancer. Cancer Res. *65*, 7065–7070.

Jeronimo, C., Forget, D., Bouchard, A., Li, Q., Chua, G., Poitras, C., Thérien, C., Bergeron, D., Bourassa, S., Greenblatt, J., et al. (2007). Systematic analysis of the protein interaction network for the human transcription machinery reveals the identity of the 7SK capping enzyme. Mol. Cell *27*, 262–274.

Kasinski, A.L., and Slack, F.J. (2011). Epigenetics and genetics. MicroRNAs en route to the clinic: progress in validating and targeting microRNAs for cancer therapy. Nat. Rev. Cancer *11*, 849–864.

Kawamata, T., and Tomari, Y. (2010). Making RISC. Trends Biochem. Sci. *35*, 368–376.

Kawamata, T., Yoda, M., and Tomari, Y. (2011). Multilayer checkpoints for microRNA authenticity during RISC assembly. EMBO Rep. *12*, 944–949.

Klose, R.J., and Bird, A.P. (2006). Genomic DNA methylation: the mark and its mediators. Trends Biochem. Sci. *31*, 89–97.

Kouzarides, T. (2007). Chromatin modifications and their function. Cell *128*, 693–705.

Kozomara, A., and Griffiths-Jones, S. (2011). miRBase: integrating microRNA annotation and deep-sequencing data. Nucleic Acids Res. *39*(Database issue), D152–D157.

Lee, Y., Ahn, C., Han, J., Choi, H., Kim, J., Yim, J., Lee, J., Provost, P., Råd-mark, O., Kim, S., and Kim, V.N. (2003). The nuclear RNase III Drosha initiates microRNA processing. Nature *425*, 415–419.

Liu, R., Wang, X., Chen, G.Y., Dalerba, P., Gurney, A., Hoey, T., Sherlock, G., Lewicki, J., Shedden, K., and Clarke, M.F. (2007). The prognostic role of a gene signature from tumorigenic breast-cancer cells. N. Engl. J. Med. *356*, 217–226.

Nakagawa, A., Shi, Y., Kage-Nakadai, E., Mitani, S., and Xue, D. (2010). Caspase-dependent conversion of Dicer ribonuclease into a death-promoting deoxyribonuclease. Science *328*, 327–334.

Park, J.E., Heo, I., Tian, Y., Simanshu, D.K., Chang, H., Jee, D., Patel, D.J., and Kim, V.N. (2011). Dicer recognizes the 5′ end of RNA for efficient and accurate processing. Nature *475*, 201–205.

Sachdeva, M., Zhu, S., Wu, F., Wu, H., Walia, V., Kumar, S., Elble, R., Watabe, K., and Mo, Y.Y. (2009). p53 represses c-Myc through induction of the tumor suppressor miR-145. Proc. Natl. Acad. Sci. USA *106*, 3207–3212.

Sarnow, P., Jopling, C.L., Norman, K.L., Schütz, S., and Wehner, K.A. (2006). MicroRNAs: expression, avoidance and subversion by vertebrate viruses. Nat. Rev. Microbiol. *4*, 651–659.

Shi, B., Sepp-Lorenzino, L., Prisco, M., Linsley, P., deAngelis, T., and Baserga, R. (2007). Micro RNA 145 targets the insulin receptor substrate-1 and inhibits the growth of colon cancer cells. J. Biol. Chem. *282*, 32582–32590.

Shuman, S. (2007). Transcriptional networking cap-tures the 7SK RNA 5′-gamma-methyltransferase. Mol. Cell *27*, 517–519.

Spizzo, R., Nicoloso, M.S., Lupini, L., Lu, Y., Fogarty, J., Rossi, S., Zagatti, B., Fabbri, M., Veronese, A., Liu, X., et al. (2010). miR-145 participates with TP53 in a death-promoting regulatory loop and targets estrogen receptor-alpha in human breast cancer cells. Cell Death Differ. *17*, 246–254.

Thomson, J.M., Newman, M., Parker, J.S., Morin-Kensicki, E.M., Wright, T., and Hammond, S.M. (2006). Extensive post-transcriptional regulation of microRNAs and its implications for cancer. Genes Dev. *20*, 2202–2207.

Xhemalce, B., and Kouzarides, T. (2010). A chromodomain switch mediated by histone H3 Lys 4 acetylation regulates heterochromatin assembly. Genes Dev. *24*, 647–652.

Xhemalce, B., Dawson, M.A., and Bannister, A.J. (2011). Histone Modifications. Encyclopedia of Molecular Cell Biology and Molecular Medicine (Hoboken, NJ: Wiley).

Zhang, H., Hao, Y., Yang, J., Zhou, Y., Li, J., Yin, S., Sun, C., Ma, M., Huang, Y., and Xi, J.J. (2011). Genome-wide functional screening of miR-23b as a pleiotropic modulator suppressing cancer metastasis. Nat. Commun. *2*, 554.

EXTENDED EXPERIMENTAL PROCEDURES

BCDIN3D Expression and Purification

BCDIN3D ORF was cloned into pGEX-5X-1 in frame with a GST tag or into pQE32 in frame with a 6xHis tag. The BCDIN3D D72A, G74A, and D72G74A mutations were introduced by site directed mutagenesis. The resulting GST and His tag fusion recombinant proteins were used in in vitro methyltransferase assays. Only the D72G74A mutation abolished the methyltransferase activity of BCDIN3D.

Cell lines

MCF-7 and MDA-MB-231 cells were purchased from ATCC and were grown in DMEM supplemented with 10% fetal bovine serum (FBS), 100 U/ml penicillin, 100 μg/ml streptomycin and 2 mM L-glutamine (PSQ). The HeLa-S3-Flp-In parental cells were constructed by using the Flp-In system from Invitrogen. Isogenic HeLa-S3-Flp-In cell lines containing a C-terminally Flag Tagged BCDIN3D construct inserted to a single site were constructed according to the protocol provided with the Flp-In system. The HeLa-S3-Flp-In cells were grown in spinner flasks at 75 rpm in RPMI+10%FBS+PSQ supplemented with 200 μg/ml of Zeocin (parental) or 400 μg/ml hygromycin (BCDIN3D-Flag).

Immunofluorescence

Cells were grown in slide flasks, washed twice with 1 ml of PBS, fixed with 5% Formalin solution in PBS for 10 min at RT, washed three times with 1 ml of PBS and permeabilized with 1 ml of PBS+3%BSA+0.6% Triton for 10 min at RT. The fixed cells were incubated O/N at 4°C with 1 ml of PBS+3%BSA and the primary antibodies and for 1 hr at RT with DAPI and the appropriate secondary antibodies. Images were acquired with an Olympus FV1000 Upright confocal microscope and processed with Adobe Photoshop CS software.

siRNA Transfection

MCF-7 and MDA-MB-231 cells were reverse transfected in two rounds with 10 or 20 nM of Dharmacon ON-TARGETplus siRNAs against BCDIN3D and control by using Lipofectamine RNAiMAX from Invitrogen or HiPerfect from QIAGEN according to the manufacturers' instructions. The siRNAs sequences are listed in Table S1.

Cellular Assays

For Soft Agar Colony assays, 3×10^4 cells from two independent clones of MDA-MB-231[shBCDIN3D] and MDA-MB-231[shNC] cell lines were imbed in 4 ml of 0.35% agar in DMEM+10%FBS+PSQ+Puromycin and plated over a 4 ml layer of 0.7% agar in the same media in a well of a 6-well plate in duplicates. Colonies were analyzed 4–5 weeks after the initial plating. For growth assays, 0.5×10^3 and 1×10^4 cells were plated in 96-well plates immediately after the second round of siRNA transfection in 6 replicates. Growth was analyzed 72 hr later with the Vybrant MTT Cell Proliferation Assay Kit (V13154) from Invitrogen according to the manufacturer's instructions. For migration and invasion assays, cells were reverse transfected in two rounds with siBCDIN3D and siNC. 48 hr after the second transfection, cells were trypsinised, counted and used in triplicates in the CytoSelect 24-well Cell Migration and Invasion assay (8 μm, Colorometric Format, CBA-100-C from Cell Biolabs, Inc) according to the manufacturer's instructions. The migration and invasion were assessed after 24 hr incubation. The real-time growth, migration and invasion assays were performed with the xCELLigence system from Roche (http://www.nature.com/nmeth/journal/v6/n8/full/nmeth.f.263.html) A total of 1×10^4 cells in DMEM+10%FBS+PSQ were plated per well in the E-plate for the growth assays, and 6×10^4 cells in DMEM+PSQ were plated per well in the upper chamber and DMEM+10%FBS+PSQ was the attractant in the lower chamber of the CIM-plate for the migration and invasion assays. 1/40 dilution of Matrigel was used to coat the upper chamber of the CIM plate for the invasion assays. All assays were performed in quadruplets and followed for 48 hr.

RNA/Protein Extraction

Total RNA and protein extraction was typically performed on ~5×10^5 cells by using the RNA/Protein purification kit from Norgen (Product no. 23000). Cells grown on 6 cm diameter dishes were washed with 5 ml of PBS and lysed with 350 μl of Lysis Buffer supplemented with 10 μl of β-mercaptoethanol per ml for 5 min on a rocking table. RNA extraction, including DNase treatment, was performed according to the manufacturer's instructions. The whole flow-through after the RNA binding step was used for protein purification. The RNA and protein concentrations were measured with a NanoDrop (ND-1000) Spectrophotometer.

RNA Clean-Up

After various in vitro enzymatic treatments, the resulting RNAs were purified by using the QIAGEN RNeasy MinElute Cleanup Kit with a modified protocol that allows recovery of RNAs of all sizes, as per the Illumina Directional mRNA-Seq Library prep. V1.0 kit Pre-Release Protocol. Briefly, each reaction was toped to 100 μl with water and mixed with 350 μl of RLT buffer and 625 μl of 100% Molecular grade Ethanol. The mixture was passed through the QIAGEN RNeasy MinElute column. The increased ratio of ethanol allows low molecular weight RNA to bind to the column. The column was successively washed with 500 μl of RPE buffer and 750 μl of 80% Ethanol, dried by centrifugation and the RNA was eluted with 20 μl of water. The validity of this method was confirmed by analysis of the RNAs on an Agilent Total Eukaryotic RNA Pico Chip and qRT-PCR.

RNA Analysis

500 ng of total RNA was used for cDNA synthesis with the SuperscriptIII First-Strand Synthesis System for RT-PCR (Invitrogen) with both oligo(dT)$_{20}$ and random hexamers. Subsequently, 1/20th of each reaction was used for PCR with gene specific primers; 20–200 ng of total RNA was used for detection of miRNAs with the *mir*Vana qRT-PCR miRNA detection kit and/or the Taqman MicroRNA Reverse Transcription Kit from Applied Biosystems. In the –RT samples, water was used instead of the reverse transcription enzymes. Real-time PCR analysis was performed on a StepOne Plus system or Vii7A from Applied Biosystems. The sequences of the primers used for PCR analysis are listed in Table S2. The northern blots were performed as previously described (Xhemalce and Kouzarides, 2010).

RNA Library Preparation and Sequencing

1 μg of total RNA was amplified with the use of the Illumina Directional mRNA-Seq Library prep. V1.0 kit, without prior poly-A enrichment, according to the manufacturer's instructions (Pre-Release Protocol). The libraries were sequenced with Small RNA sequencing primer (part no. 1001375) and the Single Read Sequencing Protocol.

In Vitro RNA Methyltransferase Assay

These assays were performed in a total volume of 100 μl in 25 mM Tris-HCl, pH8, 150 mM NaCl, 2 mM KCl, 10% glycerol, 1 mM EDTA, 1 mM DTT supplemented with EDTA-free Complete Protease Inhibitor cocktail from Roche and 80 U of RNaseOUT from Invitrogen with 1 μg of recombinant BCDIN3D, 4 μl of 20 μM RNAs and 4 μl of ^{3}H-SAM (PerkinElmer NET155250UC) for 2 hr at 37°C. The RNAs were purified by using the QIAGEN RNeasy MinElute Cleanup Kit with a modified protocol that allows recovery of RNAs of all sizes (see above). Where indicated, the samples were separated on SDS-PAGE or Urea-PAGE gels, fixed in 45% Methanol, 10% Acetic Acid, treated for 30 min with Enlightning (PerkinElmer), dried and exposed on film at −80°C.

Terminator 5′-Phosphate-Dependent Exonuclease Treatment Coupled to qRT-PCR

2 μg of total RNA was used per reaction. The Terminator treatment was performed in a total volume of 20 μl in 1X Terminator Reaction A buffer with 20 U of RNaseOUT from Invitrogen and 1 U of Terminator 5′-Phosphate-Dependent Exonuclease from Epicenter for 2 hr at 30°C. In the no Terminator treatment, water was used instead of the enzyme. The RNA was purified by using the QIAGEN RNeasy MinElute Cleanup Kit with a modified protocol that allows recovery of RNAs of all sizes (see above). After elution with 20 μl of water, 1 to 4 μl of the resulting RNAs were used for the subsequent reverse transcription and real-time or semiquantitative PCR steps.

BCDIN3D Coimmunoprecipitation

2.10^{7} HeLa-S3-FlpIn and HeLa-S3-FlpIn-BCDIN3D-Flag cells grown at a density of 4–5.10^{5} cells per ml were used per Co-IP. The cells were washed twice with 25 ml of cold PBS, extracted with 0.6 ml of cold co-IP buffer (20 mM HEPES (pH 7.5), 150 mM NaCl, 20% glycerol, 0.1% NP40, 1 mM EDTA, 0.1 mM PMSF supplemented with EDTA-free Complete Protease Inhibitor cocktail from Roche) for 1 hr at 4°C and cleared by centrifugation for 5 min at 13,000 rpm at 4°C. The supernatant was incubated for 4 hr with 40 μl of pre-washed anti Flag M2 conjugated beads (Sigma) at 4°C. The beads were washed three times with 0.5 ml of co-IP buffer, once with 0.5 ml of TBS, and eluted with 100 μl of TBS containing 150 ng/μl of 3xFlag peptide for 30 min at 4°C. The proteins were precipitated with TCA, resuspended in 20 μl of 1x Laemmli Buffer and analyzed by western blot or Coomassie as indicated. For the treatments with RNase A, the co-IPs were performed in the presence of 1 of 5 μl of RNase A solution (R6148) from Sigma.

Western Blot

Proteins were separated in SDS-PAGE gel and transferred onto 0.45 μM nitrocellulose membrane in 1X Towbin Buffer with 20% Methanol and 0.02% SDS for 90 min at 300 mA. The membranes were blocked for 30–60 min at room temperature in TBS-TM (Tris-buffered saline, 0.1% Tween 20, 5% Nonfat Dry Milk from Cell Signaling no. 9999) and incubated overnight at 4°C with TBS-TM buffer containing the indicated antibodies. The membranes were washed three times 10 min with TBS-T, incubated 1 hr with TBS-T containing the appropriate secondary antibodies, washed and revealed with ECL (Amersham). The ECL signal was detected and analyzed on film or with the Chemidoc XRS+ system from Biorad. The western blots against BCDIN3D were performed according to the BCDIN3D antibody supplier's (Sigma) instructions. The catalog and lot numbers of the commercially available antibodies used are listed in Table S3.

RNA Immunoprecipitation

Cells grown in 10 cm diameter dishes were washed with 10 ml of PBS, fixed with 10 ml of 1% formaldehyde (Sigma) in PBS for 10 min and quenched with 20 mM Glycine for 5 min. Cells were washed Twice with 10 ml of cold PBS, scraped with 2.5 ml of cold PBS supplemented with Complete Protease Inhibitor cocktail from Roche and pelleted by centrifugation. The pellet was suspended in 0.4 ml of cold RIPA Buffer (25 mM Tris-HCl, pH 7.5, 150 mM NaCl, 1 mM EDTA, 1% NP-40, 0.5% Sodium Deoxycholate, 0.05% SDS) supplemented with EDTA-free Complete Protease Inhibitor cocktail from Roche and 400 U/ml of RNaseOUT from Invitrogen. The suspension was sonicated in 2 ml tubes for 5 min at High, 30 s ON/OFF cycles in a cooled Bioruptor (Diagenode) and cleared by centrifugation for 15 min at 13,000 rpm. The supernatant was incubated with the appropriate antibodies O/N at 4°C, then with 25 μl of pre-washed Protein G Dynabeads (Invitrogen) for 3 hr at 4°C. The beads were washed five times on ice with 1 ml of High

Stringency RIPA buffer (25 mM Tris-HCl, pH 7.5, 1 M NaCl, 1 mM EDTA, 1 M Urea, 1% NP-40, 1% Sodium Deoxycholate, 0.1% SDS, 0.2 mM phenylmethylsulfonyl fluoride). The immuno-complexes were eluted from the beads with 100 µl of elution buffer (50 mM Tris–Cl, pH 7.0, 5 mM EDTA, 10 mM dithiothreitol (DTT), 1% SDS) for 1 hr at 70°C. The eluates were purified and DNase-treated with the miRNeasy Purification kit from QIAGEN and the RNA was eluted from the columns with 50 µl of water.

In Vitro Dicer Processing Assays

100 pmol of synthetic pre-miR-145 (5′OH, 5′P, 5′Pme1 or 5′Pme2) were incubated with 500 ng of recombinant human Dicer in a total volume of 15 µl in 100 mM KCl, 10 mM Tris-HCl (pH 8), 0.1 mM EDTA, 0.5 or 1 mM MgCl₂, 0.5 mM dTT supplemented with 0.5 U/µl RNaseOUT for the indicated times at 37°C. The samples were mixed with 15 µl of Gel Loading Buffer II (Ambion), heated for 15 min at 70°C and separated on a 15% Urea-PAGE. The gels were stained for 15 min with 10 µg/ml ethidium bromide and the signal was detected and analyzed with the Chemidoc XRS+ system from Biorad.

Bioinformatic Analysis

Mapping

Total RNA from siBCDIN3D- and siNC-treated MCF7 cells were sequenced by using an Illumina Genome Analyzer II, resulting in 14,558,834 and 13,512,809 reads respectively, each having a read-length of 41 bp. Reads were mapped to the human reference genome (build 37) by using TopHat (Trapnell et al., 2009), which incorporates mapping across exon-exon boundaries for RNA-seq data. The resulting genome mappings were filtered to remove nonunique mappings and reads mapped with 3 or more mismatches or gaps. This resulted in 1,163,459 and 1,276,255 unique mappings for the siBCDIN3D- and siNC-treated samples respectively. The relatively low proportion of reads with corresponding mappings is likely due to the presence of large quantities of ribosomal RNA present in the total RNA samples used for the library generation (see above). Mapped regions were extended to 200bp to more closely represent the fragment lengths.

Differential Expression

The h19 knownGene table from the UCSC genome browser (http://genome.ucsc.edu/) contains genome coordinates for 77,614 predicted genes from a variety of resources (RefSeq, GenBank, CCDS and Uniprot). For each predicted gene, the number of reads per kilobase exon model per million mapped reads (RPKM) was calculated by dividing the total number of overlapping reads in the coding portion by the total number of coding bases (in kilobases), and then normalizing this by the total number of millions of reads generated for each sample. The RPKM value was used as a proxy for the level of transcription. Differential expression between siBCDIN3D- and siNC-treated samples was calculated by using the DESeq package in R (Anders and Huber, 2010). Genes showing a significant change in expression were selected based on a fold-change greater than 2 between the two samples and a p value from the negative binomial model fitting less than 0.05, an mRNA length greater than 500 bp and a normalized read count greater than 100 for at least one of the samples.

Identification of miRNA binding to the 3′-UTR of known genes

Potential miRNA target predictions were taken from the microRNA.org repository (http://www.microRNA.org), which used an updated version of the miRanda algorithm to find miRNA binding sites in known genes (Betel et al., 2008). The August 2010 release of human target site predictions (human_predictions_S_C_aug2010.txt) was used. All entries with an alignment score less than 150 and a mirSvr score greater than −0.5 were removed to avoid potentially false binding sites. Genes were partitioned into classes based on whether or not the fold change was significant, and whether or not at least one miRNA was detected with a potential binding site in the 3′ UTR of the gene. The significance of whether genes with significant fold change (up, down, or either) were enriched for potential regulation by miRNAs was calculated by performing a Fisher's Exact Test on the 2 × 2 contingency table. miRNAs significantly enriched within the 3′ UTR of significantly changing genes (up, down, or either) were identified by estimating an expected count based on the proportion of occurrences across all nonsignificant genes and performing a chi-square test on the observed counts.

MicroRNA Profiling

Total RNA from MCF-7 cells treated with siBCDIN3D or siNC from two fully independent experiments were submitted to miRNA profiling by miRCURY LNA Universal RT miRNA PCR Human panel I and II v2 (742 assays total) from Exiqon. The integrity of RNA was verified by electrophoresis on a Agilent Total Eukaryotic RNA Nano Chip. Furthermore, the RNA quality control by qPCR did not detect presence of inhibitors in the samples. All microRNAs were polyadenylated and reverse transcribed into cDNA in a single reaction step. cDNA and SYBR Green mastermix were transferred to qPCR panels preloaded with primers, using a pipetting robot. Amplification was performed in a Roche Lightcycler480. Raw crossing point (Cp) values and melting points, as detected by the Light cycler software, were exported. The data sets were cleared from: (1) reactions with several melting points; (3) reactions with melting points that were not within assay specifications; (3) reactions with amplification efficiency below 1.6; (4) reactions giving Cp values that were within 5 Cp values of the negative controls reaction; (5) reactions with Cp > 37. In addition, only the assays that showed good quality signal in all samples were further analyzed. Each assay within a sample was then normalized to the average of the assays within the sample with the formula:

$$\text{Normalized Cp} = \text{average}(n = 110) - \text{assay Cp}$$

The averages and variances for siBCDIN3D and siNC groups were calculated, and in order to eliminate false positives, the assays with a variance higher than 50% of the absolute average were discarded. Then, the average Cp of the siNC group was subtracted from the average Cp of the BCDIN3D group with the formula:

$$ddCp = \text{Normalized Cp}[\text{siNC}] - \text{Normalized Cp}[\text{siBCDIN3D}]$$

The resulting values represent the difference in miRNA expression (log2 scale), with positive values representing upregulation in siBCDIN3D compared to siNC and negative values downregulation.

SUPPLEMENTAL REFERENCES

Anders, S., and Huber, W. (2010). Differential expression analysis for sequence count data. Genome Biol. *11*, R106.

Betel, D., Wilson, M., Gabow, A., Marks, D.S., and Sander, C. (2008). The microRNA.org resource: targets and expression. Nucleic Acids Res. *36*(Database issue), D149–D153.

Trapnell, C., Pachter, L., and Salzberg, S.L. (2009). TopHat: discovering splice junctions with RNA-Seq. Bioinformatics *25*, 1105–1111.

Xhemalce, B., and Kouzarides, T. (2010). A chromodomain switch mediated by histone H3 Lys 4 acetylation regulates heterochromatin assembly. Genes Dev. *24*, 647–652.
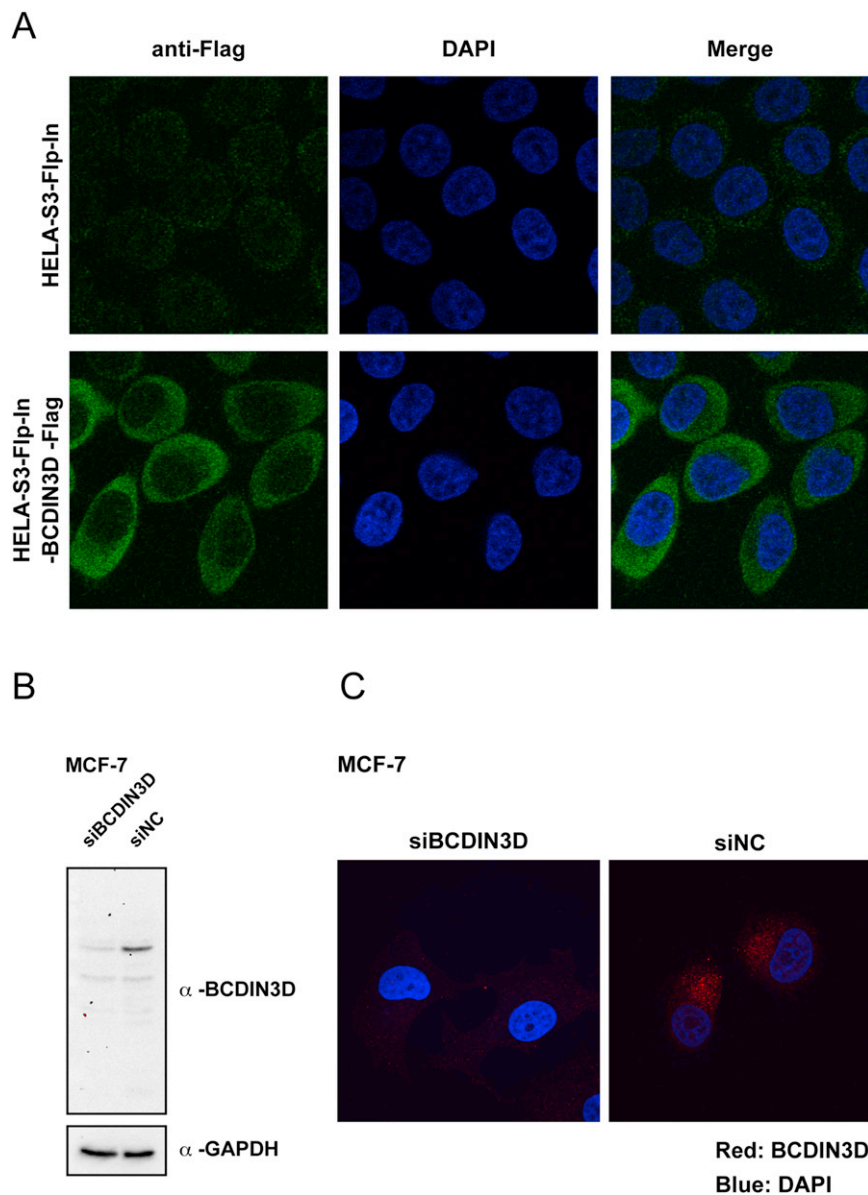
Figure S1. BCDIN3D Is Mainly Localized in the Cytoplasm, Related to Figure 1

(A) Immunofluorescence staining of isogenic HELA-S3-Flp-In and HELA-S3-Flp-In-BCDIN3D-Flag stable cell lines with an anti Flag Antibody.

(B) Whole-cell extracts from MCF-7 cells transfected with siBCDIN3D and siNC were analyzed by western blot with an antibody against BCDIN3D. The membrane was stripped and analyzed with an antibody against GAPDH to control for equal loading of the samples.

(C) Immunofluorescence staining of MCF-7 cells with the anti BCDIN3D antibody (same as in B).

Figure S2. siRNA-Mediated Depletion of BCDIN3D Suppresses Tumorigenic Phenotypes In Vitro, Related to Figure 2

(A–D) BCDIN3D depletion suppresses the invasiveness of the MDA-MB-231 cells, without affecting their growth and migration abilities. MDA-MB-231 cells were transfected with siBCDIN3D and siNC, and their growth (A, *MTT assay*), ability to migrate through a 8 μM pore size membrane (B, *Migration assay*) or to invade a 8 μM pore size membrane coated with dried basement membrane matrix solution (C&D, *Invasion assay*) were tested in parallel (see Extended Experimental Procedures for further detail). Error bars represent SEM values.
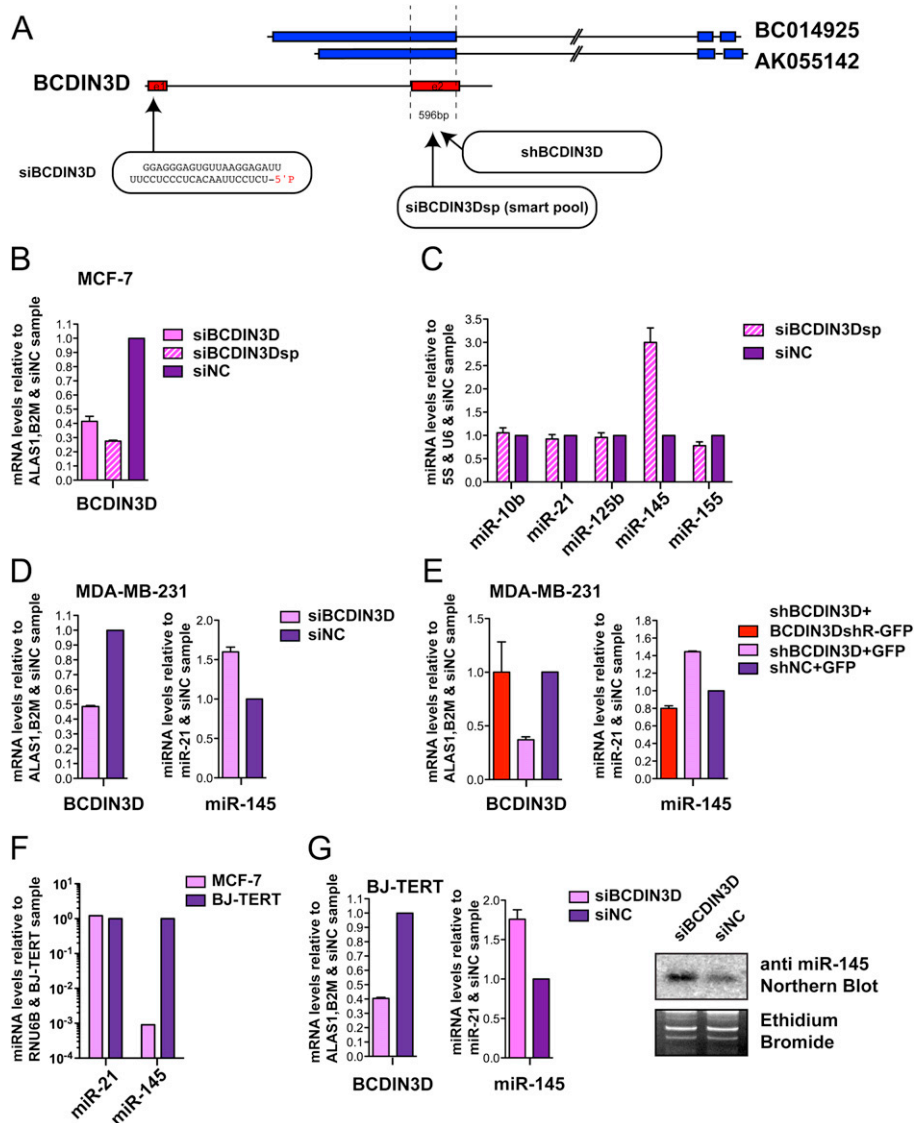
Figure S3. Depletion of BCDIN3D Increases the Levels of Mature miR-145 in Several Cell Lines, Related to Figure 3

(A) Schematic view of the BCDIN3D gene locus. The BCDIN3D gene contains 2 exons. The sequence of the siRNA targeting the first exon of BCDIN3D is shown. The shRNA as well as the smart pool of siRNAs against BCDIN3D targets the second exon. The second exon contains 596 bp complementarity to two non coding RNAs that are transcribed in the opposite direction to the BCDIN3D gene. The siRNAs were ordered as ON-TARGETplus siRNAs from Dharmacon, where only the antisense oligonugleotide is 5′ monophosphorylated in order to minimize the effect of these siRNAs on the noncoding RNAs.

(B) MCF-7 cells were transfected with the siRNA targeted against the first exon of BCDIN3D (siBCDIN3D) or the pool of siRNAs targeted against the second exon of BCDIN3D (siBCDIN3Dsmartpool) or with non targeting siRNAs as a negative control (siNC). BCDIN3D mRNA levels from these cells were analyzed by quantitative Reverse Transcription and PCR analysis (qRT-PCR) and normalized to the ALAS1 and B2M mRNAs and to siNC cells. Error bars represent SEM values.

(C) MCF-7 cells were transfected with siBCDIN3Dsmartpool or with siNC and the levels of the indicated mature miRNA were analyzed. The data are normalized to 5S and the U6 RNA and to miRNA levels in the siNC-treated cells. Error bars represent SEM values.

(D) MDA-MB-231 cells were transfected with siBCDIN3D and siNC and the levels of BCDIN3D, miR-21, miR-145 were analyzed by qRT-PCR. The BCDIN3D mRNA levels were normalized to the ALAS1 and B2M mRNAs and to siNC cells, while the miR-145 levels were normalized to the miR-21 RNA and to miRNA levels in the siNC-treated cells. Error bars represent SEM values. NB. In depth analysis of several other miRNAs, as well as small RNAs broadly used to normalize levels of miRNAs, such as 5S, U6 and RNU6B, revealed that using miR-21 to normalize miR-145 levels is a more appropriate method even though it underestimates the apparent increase in the levels of miR-145 in siBCDIN3D versus siNC cells.

(E) RNA from MDA-MB-231 [shBCDIN3D+BCDIN3DshR(esistant)-GFP], MDA-MB-231 [shBCDIN3D+GFP] and MDA-MB-231 [shNC+GFP] cell lines was analyzed as in (D).

(F) BJ+hTERT cells express significantly higher levels of miR-145 than MCF-7 cells. The levels of miR-21 and miR-145 from MCF-7 and immortalized human embryonic fibroblasts BJ+hTERT were analyzed by qRT-PCR and normalized to the RNU6B RNA and to BJ+hTERT cells. Error bars represent SEM values.

(G) RNA from BJ-TERT cells transfected with siBCDIN3D and siNC was analyzed as in (D), as well as by northern blot with a probe against miR-145.
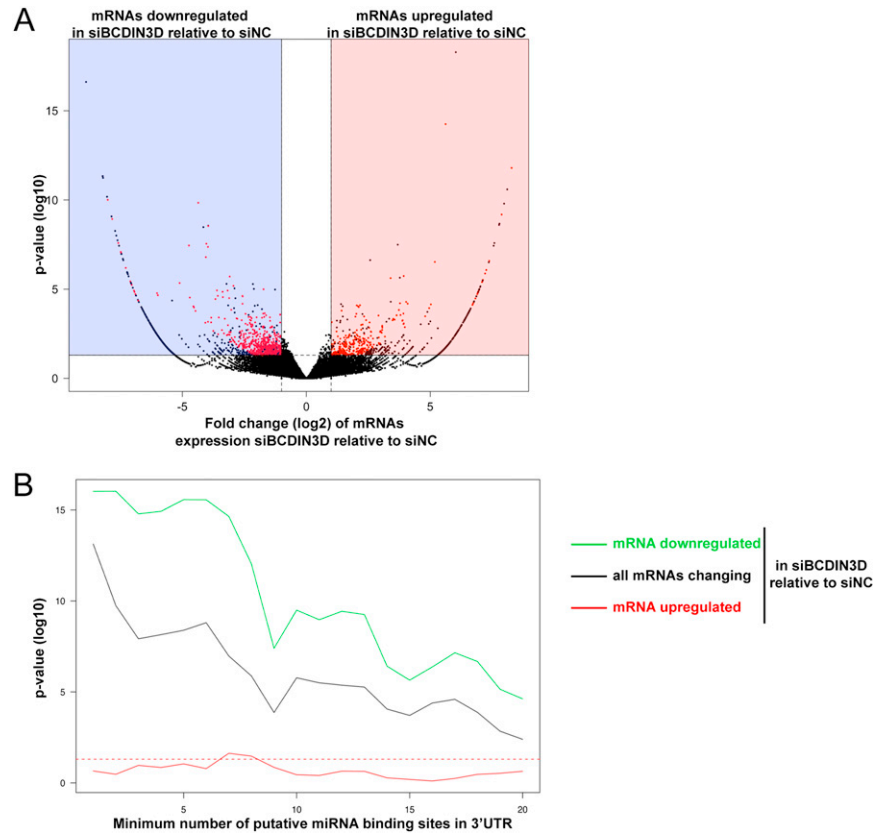
Figure S4. miRNA Motifs Are Significantly Enriched in the 3′UTR of Genes Downregulated upon BCDIN3D Depletion, Related to Figure 5

Total RNA from MCF-7 cells transfected with siBCDIN3D and siNC was amplified, sequenced and analyzed as indicated in the Extended Experimental Procedures.

(A) Volcano plot representation of the fold change of normalized mRNA read counts between siBCDIN3D- and siNC-treated samples (x axis, log2) and the p value allocated to the fold change (y axis, log10). Red points indicate significantly downregulated or upregulated genes based on fold change greater than 2, p value equal to or lower than 0.05, mRNA exonic length higher than 500 bases and normalized read count greater than 100 for at least one of the samples.

(B) The 3′UTRs of significantly downregulated or upregulated genes between siBCDIN3D- and siNC- samples were analyzed for the presence of putative miRNA regulatory sequences as indicated in the Extended Experimental Procedures. A Fisher's exact test was performed to calculate the p value (y axis, log10) associated with the likelihood of a given number of miRNA (x axis) to be present more than expected in the 3′ UTR of mRNAs that are either downregulated (green line), upregulated (red line) or changing (sum of dowregulated and upregulated, black line) in siBCDIN3D versus siNC. The red dashed line corresponds to the p = 0.05 threshold.
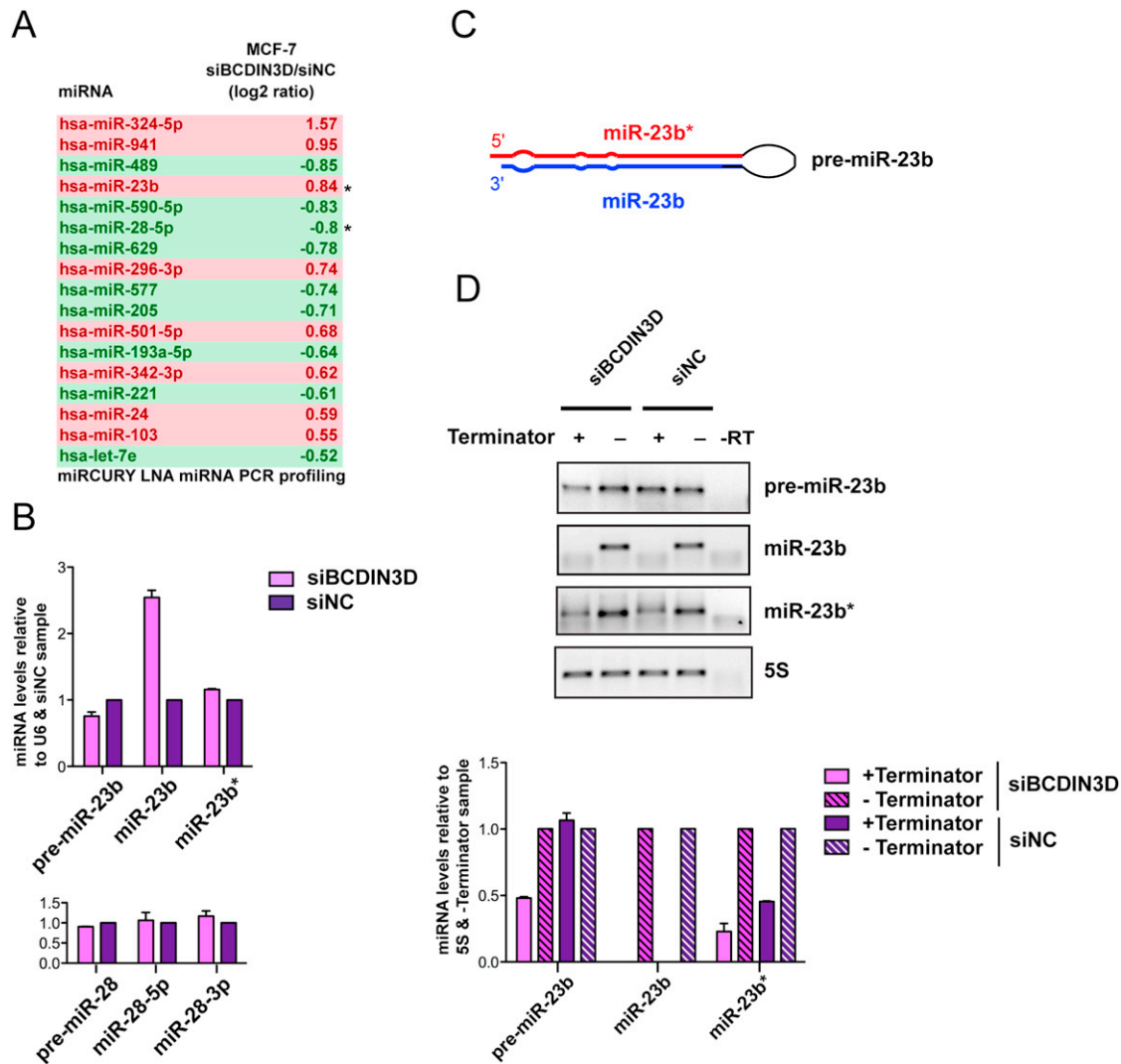
Figure S5. BCDIN3D Regulates Other miRNAs, Related to Figure 5

(A) Total RNA from MCF-7 cells treated with siBCDIN3D or siNC were submitted to miRNA profiling by miRCURY LNA Universal RT miRNA PCR (Exiqon) (see Extended Experimental Procedures for further detail). The list represents miRNAs whose expression was found significantly increased (red), or decreased (green) by a log2 ratio superior to 0.5 or inferior to −0.5, respectively, by the miRNA PCR profiling procedure. To present, we have not been able to validate the decrease of several of the miRNAs shown in green (miR-28, S5B and data not shown). This could be due to the fact that we normalized the data to the mean expression of all miRNAs in each sample and the overall expression of miRNAs was increased in siBCDIN3D compared to siNC samples (Extended Experimental Procedures). However, we were able to validate the overexpression of several miRNAs shown in red (miR-23b, B and data not shown).

(B) MCF-7 cells were transfected with siBCDIN3D and siNC and the levels of the precursor, mature and passenger strand of miR-23b and miR-28 were analyzed by quantitative Reverse Transcription and PCR (qRT-PCR) analysis. The data are normalized to the U6 RNA and to siNC cells. Error bars represent SEM values. Similar results were obtained in MDA-MB-231 cells thereby validating miR-23b as a good candidate for siBCDIN3D-dependent regulation.

(C) Pre-miR-23b and miR-23b* share the same 5′end. Schematic showing the position of miR-23b and miR-23b* within the pre-miR-23b hairpin.

(D) pre-miR-23b, and to a lesser extent, miR-23b* are modified in a BCDIN3D-dependent manner. RNA from MCF-7 cells transfected with siBCDIN3D and siNC were treated or not with Terminator 5′-P-dependent exonuclease as in Figure 5, and further analyzed by Reverse Transcription and semiquantitative PCR with the indicated primers (upper panels). All the indicated RNAs were also analyzed by quantitative RT-PCR (lower graph). The data are normalized to the 5S RNA and to the [- Terminator] sample. Error bars represent SEM values.
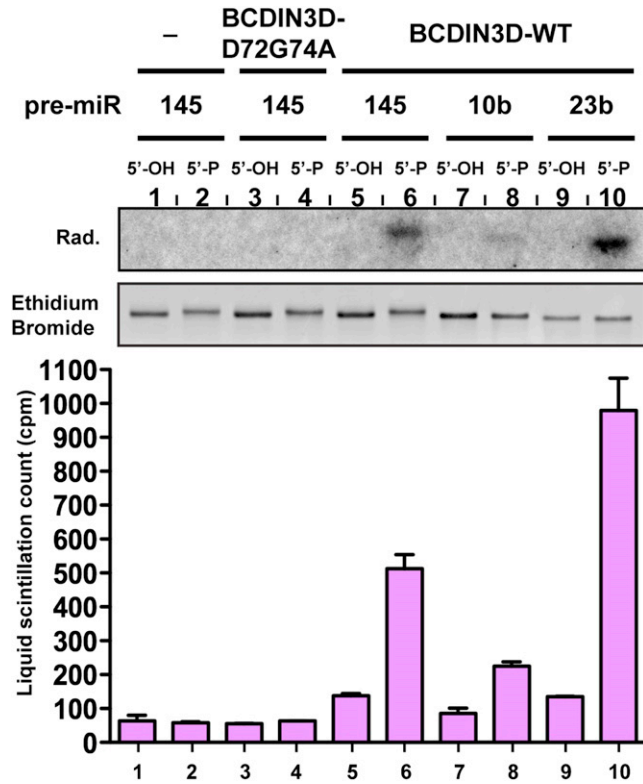
Figure S6. BCDIN3D Methylates Other Pre-miRNAs In Vitro, Related to Figure 5

In vitro methyltransferase assay using mock (1–2), recombinant BCDIN3D (5–10) or recombinant BCDIN3D-D72G74A (3–4), ^{3}H-radioactive SAM as methyl group donor and the following synthetic RNA molecules as substrate (1, 3, 5) pre-miR-145 [5′-OH]; (2, 4, 6) pre-miR-145 [5′-P]; (7) pre-miR-10b [5′-OH]; (8) pre-miR-10b [5′-P]; (9) pre-miR-23b [5′-OH]; (10) pre-miR-23b [5′-P]. The nucleic acids were purified and analyzed by autoradiography (panels, the lower panel shows the Staining with ethidium bromide of the gel used for the autoradiography shown in the upper panel) and liquid scintillation (graph). Error bars represent SD values.
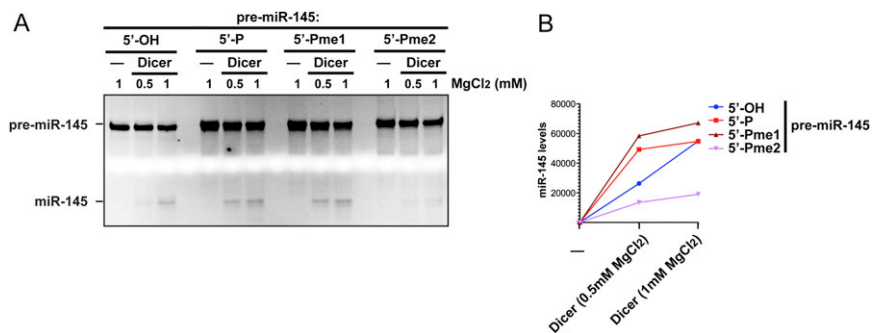
Figure S7. Phospho-Dimethylated Pre-miR-145 Is Poorly Processed by Human Dicer In Vitro, Related to Figure 6

Synthetic pre-miR-145 molecules that have [5′-OH], [5′-P], [5′-Pme1] or [5′-Pme2] 5′ ends were incubated with human Dicer or mock at the indicated concentrations of MgCl$_2$ (see Extended Experimental Procedures for further detail). The Dicer processing reactions were loaded on a 15% Urea-PAGE gel and stained with ethidium bromide. The gel was photographed with the Chemidoc XRS+ system from Biorad and the miR-145 product was quantified by using the Image Lab Software.

Table S1. List of siRNAs, premiR Mimics and Inhibitors, Related to the Experimental Procedures

siRNA	Target Sequence
ON-TARGETplus siBCDIN3D_exon1	GGAGGGAGUGUUAAGGAGA
ON-TARGETplus SMARTpool L-018768-02-0005, hBCDIN3D	CUGCAAGGCGUCUCCGAAA
	ACAAUCAGGCAGCCGCAAA
	ACGUGGAAAUCCCAUCAAA
	CUUCAAGAGAAUUCCGUCU
ON-TARGETplus Non-targeting Pool D-001810-10-05	Not provided by the supplier
Pre-miR™ miRNA Precursor- hsa-miR-145-5p	Ambion
Pre-miR™ miRNA Precursor-Negative Control #1	Ambion
*mir*Vana® miRNA inhibitor- hsa-miR-145-5p	Ambion
*mir*Vana® miRNA inhibitor- Negative Control #1	Ambion

Table S2. List of Oligonucleotides, Related to the Experimental Procedures

Primers	Code	Sequence /Supplier
hBCDIN3D_FWD	TK08234	GCCCCGTTCGGAAATTTTC
hBCDIN3D_REV	TK08235	ACACTCAGATCCCCGGAGTTAC
hIRS1_FWD	TK10907	AGAGGACCGTCAGTAGCTCAAC
hIRS1_REV	TK10908	TTTCGCTTGGCACAATATAGAA
hALAS1	Hs_ALAS1_1_SG	Qiagen QuantiTect® Primer Assay QT00073122
hB2M	Hs_B2M_1_SG	Qiagen QuantiTect® Primer Assay QT00088935
pri-miR-21	Hs03302625_pri	ABI TaqMan® Pri-miRNA Assay # 4427012
pri-miR-145_FWD		AGGGCCAGCAGCAGGC
pri-miR-145_FWD		TCAGGAAATGTCTCTGGCTGTG
pre-miR-21_FWD	TK10134	TAGCTTATCAGACTGATGTT
pre-miR-21_REV	TK10135	ACAGCCCATCGACTGGTGTT
pre-miR-145_FWD	TK10132	GTCCAGTTTTCCCAGGAATC
pre-miR-145_REV	TK10133	AGAACAGTATTTCCAGGAAT
miR-21	hsa-miR-21	ABI TaqMan® MicroRNA Assay # 4373090
miR-145	hsa-miR-145	ABI TaqMan® MicroRNA Assay # 4395389
RNU6B	RNU6B	ABI TaqMan® MicroRNA Assay # 4427975
miR-10b	AM30018	Ambion mirVana™ qRT-PCR Primer Set (miR-10b)
miR-21	AM30102	Ambion mirVana™ qRT-PCR Primer Set (miR-21)
miR-125b	AM30022	Ambion mirVana™ qRT-PCR Primer Set (miR-125b)
miR-145	AM30047	Ambion mirVana™ qRT-PCR Primer Set (miR-145)
miR-155	AM30059	Ambion mirVana™ qRT-PCR Primer Set (miR-155)
5S	AM30302	Ambion mirVana™ qRT-PCR Primer Set for Normalization (5S)
U6	AM30303	Ambion mirVana™ qRT-PCR Primer Set for Normalization (U6)
Pre-miR-23b_FWD	BX00009	TGGCATGCTGATTTGTGACT
Pre-miR-23b_REV	BX000010	GGTAATCCCTGGCAATGTGA
miR-23b_FWD	BX000011	ACACTCCAGCTGGGATCACATTGCCAG
miR-23b_RT	BX000012	CTCAACTGGTGTCGTGGAGTCGGCAATTCAGTTGAGGGTAATCC
miR-23b*_FWD	BX000013	ACACTCCAGCTGGGTGGGTTCCTGGCAT
miR-23b*_RT	BX000014	CTCAACTGGTGTCGTGGAGTCGGCAATTCAGTTGAGAAATCAGC
Pre-miR-28_FWD	BX000015	GCTCACAGTCTATTGAGTTACCTTTC
Pre-miR-28_REV	BX000016	CCAGGAGCTCACAATCTAGTGG
miR-28-5p_FWD	BX000017	ACACTCCAGCTGGGAAGGAGCTCACAGT
miR-28-5p _RT	BX000018	CTCAACTGGTGTCGTGGAGTCGGCAATTCAGTTGAGCTCAATAG
miR-28-3p _FWD	BX000019	ACACTCCAGCTGGGCACTAGATTGTGAG
miR-28-3p _RT	BX000020	CTCAACTGGTGTCGTGGAGTCGGCAATTCAGTTGAGTCCAGGAG

pre-miR-145-5'OH	Synthetic RNA	5'OH – GUCCAGUUUUCCCAGGAAUCCCUUAGAUGCUAAGAUGGGGAUUCCUGGAAAUAC UGUUCU
pre-miR-145-5'P	Synthetic RNA	5'PO$_4$ – GUCCAGUUUUCCCAGGAAUCCCUUAGAUGCUAAGAUGGGGAUUCCUGGAAAUAC UGUUCU
pre-miR-145-5'Pme1	Synthetic RNA	5'PO$_4$CH$_3$ – GUCCAGUUUUCCCAGGAAUCCCUUAGAUGCUAAGAUGGGGAUUCCUGGAAAUAC UGUUCU
pre-miR-145-5'Pme2	Synthetic RNA	5'PO$_4$C$_2$H$_6$ – GUCCAGUUUUCCCAGGAAUCCCUUAGAUGCUAAGAUGGGGAUUCCUGGAAAUAC UGUUCU
miR-145-P	Synthetic RNA	5'PO$_4$ –GUCCAGUUUUCCCAGGAAUCCCU
miR-145*-P	Synthetic RNA	5'PO$_4$ –GGAUUCCUGGAAAUACUGUUCU
pre-miR-10b-5'OH	Synthetic RNA	5'OH – UACCCUGUAGAACCGAAUUUGUGUGGUAUCCGUAUAGUCACAGAUUCGAUUCU AGGGGAAU
pre-miR-10b-5'P	Synthetic RNA	5'PO$_4$ – UACCCUGUAGAACCGAAUUUGUGUGGUAUCCGUAUAGUCACAGAUUCGAUUCU AGGGGAAU
pre-miR-23b-5'OH	Synthetic RNA	5'OH – UGGGUUCCUGGCAUGCUGAUUUGUGACUUAAGAUUAAAAUCACAUUGCCAGGG AUUACC
pre-miR-23b-5'P	Synthetic RNA	5'PO$_4$ – UGGGUUCCUGGCAUGCUGAUUUGUGACUUAAGAUUAAAAUCACAUUGCCAGGG AUUACC

Table S3. List of Antibodies, Related to the Experimental Procedures

Antibody	Provider	Catalog number	Lot number
Anti-BCDIN3D	Sigma	HPA039911	R36480
Anti-IRS1	Thermo Scientific	# 1861242	# IK118947
Anti-p53	Active Motif	# 39553	# 00909001
Anti-GAPDH	Abcam	ab9485	954292
Anti-Drosha	Abcam	ab12286	552659
Anti-Dicer	Cell Signaling	# 3363	# 1
Anti-Ago2	Cell Signaling	# 2897	# 2
Anti-TRBP	Abcam	ab42018	754952
Anti-Tubulinα	Abcam	ab7291	525683
Anti-Tubulinβ	Abcam	ab6046	86729
GFP	Molecular Probes	A11122	779558
Flag	Sigma	F7425	026K4848
Flag	Sigma	F1804	124K6106
3xFlag Peptide	Sigma	F4799	